Journal of Computational Neuroscience (2019) 47:91–108
https://doi.org/10.1007/s10827-019-00724-6

Mitochondrial dysfunction and role in spreading depolarization and seizure

Patrick Toglia[1] · **Ghanim Ullah**[1]

Received: 13 July 2018 / Revised: 12 March 2019 / Accepted: 26 July 2019 / Published online: 11 September 2019

Abstract

The effect of pathological phenomena such as epileptic seizures and spreading depolarization (SD) on mitochondria and the potential feedback of mitochondrial dysfunction into the dynamics of those phenomena are complex and difficult to study experimentally due to the simultaneous changes in many variables governing neuronal behavior. By combining a model that accounts for a wide range of neuronal behaviors including seizures, normoxic SD, and hypoxic SD (HSD), together with a detailed model of mitochondrial function and intracellular Ca^{2+} dynamics, we investigate mitochondrial dysfunction and its potential role in recovery of the neuron from seizures, HSD, and SD. Our results demonstrate that HSD leads to the collapse of mitochondrial membrane potential and cellular ATP levels that recover only when normal oxygen supply is restored. Mitochondrial organic phosphate and pH gradients determine the strength of the depolarization block during HSD and SD, how quickly the cell enters the depolarization block when the oxygen supply is disrupted or potassium in the bath solution is raised beyond the physiological value, and how fast the cell recovers from SD and HSD when normal potassium concentration and oxygen supply are restored. Although not as dramatic as phosphate and pH gradients, mitochondrial Ca^{2+} uptake has a similar effect on neuronal behavior during these conditions.

Keywords Spreading depolarization · Seizures · Mitochondrial dysfunction · Ion concentrations · Volume dynamics · Hypoxia

1 Introduction

Dynamic microenvironment within the extracellular space (ECS), modified by ionic fluxes from neurons, glia, and blood vessels, plays a critical role in neuronal behavior (Somjen 2004). In particular, pathological states involving excessive neuronal depolarization such as epileptic seizure (SZ), spreading depolarization (SD), and hypoxic spreading depolarization (HSD) are characterized by significant shuffling of various ions between intracellular space and neuronal microenvironment, exchange of ions between various intracellular compartments, and cell swelling (Somjen 2004; Bikson et al. 2003; Ayata and Lauritzen 2015; Hartings et al. 2017; Dreier and Reiffurth 2015; Enger et al. 2015; Hansen and Zeuthen 1981; Ingram et al. 2013; Cressman et al. 2009; Wei et al. 2014b; Kager et al. 2000; 2007; Krishnan and Bazhenov 2011; Wei et al. 2014a; Ullah et al. 2009; Ullah et al. 2015; Hübel et al. 2017; Hübel and Ullah 2016; Hübel et al. 2016; Brisson and Andrew 2012; Andrew et al. 2017; Dreier et al. 2013; Hübel and Dahlem 2014). In each of these conditions, collapse of transmembrane ionic gradients leads to enhanced oxygen (O_2) and glucose consumption due to active transport systems to reestablish the gradients (Wei et al. 2014a; Ingram et al. 2013).

Experimentally, SZ and SD can be induced by hypoglycemia, hypoxia, neural injury, inhibition of Na^+/K^+ pumps or high concentration of K^+ in the tissue (Dreier and Reiffurth 2015; Dreier 2011; Somjen 2004; Brisson and Andrew 2012). Increasing K^+ concentration in the bath perfusate from normal 3 mM to 8 mM induces spontaneous periodic seizures (Somjen 2004; Traynelis and Dingledine 1988) and further increasing it to a range from 25 mM to

Action Editor: Maxim Bazhenov

Electronic supplementary material The online version of this article (https://doi.org/10.1007/s10827-019-00724-6) contains supplementary material, which is available to authorized users.

✉ Ghanim Ullah
gullah@usf.edu

[1] Department of Physics, University of South Florida, 4202 E. Fowler Ave., Tampa, FL 33620, USA

40 mM (Somjen 2004; Anderson and Andrew 2002; Zhou et al. 2010; Dreier et al. 2017) causes SD. HSD is observed after reduction of blood flow or O_2 (Czéh et al. 1993; Jing et al. 1994). For the purpose of this paper, we define SZ, SD, and HSD respectively as the ion concentrations-induced high-frequency bursts not usually seen in the normal condition of the same cell (Somjen 2004; Kager et al. 2000), the nearly complete depolarization of the cell's membrane potential that recovers spontaneously on the scale of seconds (Kager et al. 2000, 2002; Conte et al. 2018), and the nearly complete depolarization of the cell's membrane potential triggered by O_2 (and glucose) deprivation that recovers only after normal O_2 supply is restored (Somjen 2004; Brisson and Andrew 2012; Brisson et al. 2013; Diekman et al. 2013; Chang et al. 2013).

The depleting O_2 reserves during SZ and SD are well documented and result from the excessive use of ATP by various pumps to restore the ion gradients across plasma membrane and membranes of intracellular organelles (Ingram et al. 2013; Bahar et al. 2006; Dreier and Reiffurth 2015; Ayata and Lauritzen 2015; Galeffi et al. 2011). However, the stress experienced by mitochondria due to the high demand for ATP and the behavior of key variables regulating ATP production during these pathological states are not throughly investigated. Furthermore, the role of these key mitochondrial variables in the dynamics of SZ and SD is not well understood. During SD and HSD in particular, where the loss in ion gradients is extreme, and the balance between ATP supply and expenditure is severely strained, understanding the behavior of mitochondria becomes more important. Given that SD is associated with a range of pathological conditions including migraine, ischemic stroke, aneurysmal subarachnoid hemorrhage, intracerebral hematoma, and trauma (Lauritzen et al. 2011), and the survival of cells in several brain regions critically depends on recovery from SD (Aitken and Schiff 1986; Brisson and Andrew 2012; Brisson et al. 2013; Hartings et al. 2017; Dreier and Reiffurth 2015), understanding the role of mitochondria in the dynamics of SD is crucial. However, existing experimental techniques are too limited to investigate the wide range of variables involved in SZ and SD, and the relevant changes in mitochondrial function. To overcome this void, we develop a comprehensive model that takes into account all key variables to quantify the stress experienced by mitochondria and its role in SZ, SD, and HSD.

We expand our model that replicates neuronal behavior during SZ, SD, and HSD (Wei et al. 2014a, b; Ullah et al. 2015) and incorporate the formalism for mitochondrial function (Toglia et al. 2016; Toglia and Ullah 2016; Toglia et al. 2018) to determine how mitochondrial function is impacted during these three conditions. By incorporating neuronal membrane potential, dynamic changes in ion concentrations and cell volume, and rate equations modeling mitochondrial function into one comprehensive framework, we are not only able to investigate the effect of pathological neuronal behavior on mitochondria, but can also determine the role of certain mitochondrial variables in the recovery of neuronal ionic gradients to restore normal cell function. Using the model, we show that the significant rise in intracellular Ca^{2+} concentration observed during SZ, SD, and HSD raises mitochondrial Ca^{2+} concentration, leading to diminished mitochondrial membrane potential ($\triangle\Psi_m$) and reduced ATP production. Furthermore, we find that both organic phosphate concentration ($[P_i]$) and pH gradient across mitochondrial membrane (ΔpH) play a key role in helping neuron to recover from HSD faster. Optimal $[P_i]$ =20mM and ΔpH=-0.6 bring cellular ATP level back to resting-state value quicker, enabling ATP-dependent pumps to recover ionic gradients necessary for cellular function faster. In normoxic SD, pH gradients and $[P_i]$ affect the strength and duration of depolarization block, the interval between spontaneous SD events, the transition to SD, and recovery from SD.

2 Methods

In this section, we describe the equations modeling the dynamics of neuronal membrane potential, intra- and extracellular ion concentrations, O_2 supply, volume of the cell, and mitochondrial function. A diagram outlining the full model is shown in Fig. 1. A complete list of rate equations involved in the model is given in the supplemental information (Tables 1S and 2S).

2.1 Neuronal membrane potential and ion concentration dynamics

We use a single compartment neuronal model containing transient Na^+, delayed rectifier K^+, specific leak currents for Na^+, K^+, and Cl^-, and Na^+/K^+ pump currents in the plasma membrane (Wei et al. 2014b). The membrane potential V_m, of the neuron is modeled by modified Hodgkin-Huxley equations:

$$C_{mem}\frac{dV_m}{dt} = -I_{Cl} - I_{Na^+} - I_K - I_{pump}/\gamma, \quad (1)$$

$$I_{Na} = G_{Na}m^3h(V_m - E_{Na}) + G_{NaL}(V_m - E_{Na}), \quad (2)$$

$$I_K = G_K n^4(V_m - E_k) + G_{KL}(V_m - E_k), \quad (3)$$

$$I_{Cl} = G_{ClL}(V_m - E_{Cl}), \quad (4)$$

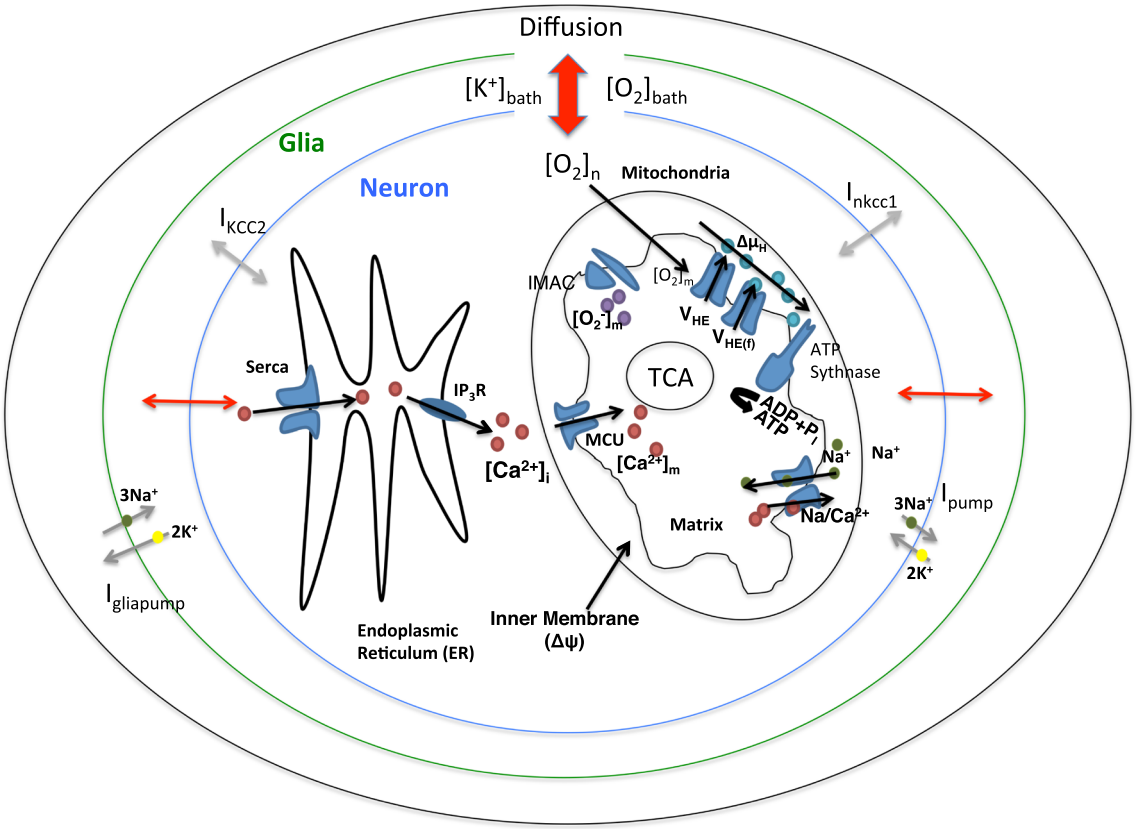

Fig. 1 Model scheme. The model incorporates the changes in neuronal volume as transmembrane osmolarity changes (thin red arrows), ATP-dependent pumps on both neuron and glia (green and yellow bullets) and diffusion of O_2 and K^+ from bath to the cell (thick red arrow). Transporters KCC2 and NKCC1 regulate intracellular Cl^-. $[O_2]$ is consumed by mitochondria through TCA cycle oxygen consumption (V_{o2}), oxidation of NADH (V_{HE}), and $FADH_2$ ($V_{HE(f)}$). Ca^{2+} is released by IP_3R or leak channels from the ER to the cytoplasm and brought back into the ER by ATP-dependent SERCA pumps. Excessive $[Ca^{2+}]_i$ is sequestered by mitochondria through the MCU and released back through Na^+/Ca^{2+} exchange. Several plasma membrane currents and other pathways are omitted from the schematic for clarity. We refer the reader to Wei et al. (2014b) and Toglia et al. (2016) for full details about the neuronal and mitochondrial models respectively

$$\frac{dm}{dt} = \alpha_m(1 - m) - \beta_m m, \tag{5}$$

$$\frac{dh}{dt} = \alpha_h(1 - h) - \beta_h h, \tag{6}$$

$$\frac{dn}{dt} = \alpha_n(1 - n) - \beta_n n. \tag{7}$$

Where G_{Na}, G_K, G_{NaL}, G_{KL}, and G_{CIL} represent maximum conductances for voltage-gated Na^+, voltage-gated K^+, Na^+ leak, K^+ leak, and Cl^- leak channels respectively. I_{pump} is the net current due to the Na^+/K^+ ATP-dependent pumps that stoichiometrically brings in two K^+ for extruding three Na^+ ions, and γ=S/(Fυ_i) is a conversation factor from the current units ($\mu A/cm^2$) into concentration units (mM/s), where S and F are the surface area of the neuron and Faraday constant respectively.

The activation and inactivation variables m, h, and n govern the fraction of voltage-gated Na^+ and K^+ channels in the active and inactive states. The parameters α_m, β_m, α_n, β_n, α_h, and β_h are the forward and backward rates for these gating variables and are adopted from a model for hippocampal pyramidal cell (Gloveli et al. 2005; Traub et al. 1994).

$$\alpha_m = 0.32(54 + V_m)/(1.0 - \exp(-(V_m + 54)/4)), \tag{8}$$

$$\beta_m = 0.28(V_m + 27)/(\exp((V_m + 27)/5) - 1), \tag{9}$$

$$\alpha_h = 0.128\exp(-(50 + V_m)/18), \tag{10}$$

$$\beta_h = 4/(1 + \exp(-(V_m + 27)/5)), \tag{11}$$

$$\alpha_n = 0.032(V_m + 52)/(1 - \exp(-(V_m + 52)/5)), \tag{12}$$

$$\beta_n = 0.5\exp(-(V_m + 57)/40). \tag{13}$$

The reversal potentials for Na^+ (E_{Na}), K^+ (E_k), Cl^- (E_{Cl}), and Ca^{2+} (E_{Ca}) currents are given by Nernst equations

where $[\bullet]_i$ and $[\bullet]_o$ represent ion concentration inside and outside the cell, respectively.

$$E_{Na} = 26.64 \ln\left(\frac{[K^+]_o}{[K^+]_i}\right), \tag{14}$$

$$E_{Na} = 26.64 \ln\left(\frac{[Na^+]_o}{[Na^+]_i}\right), \tag{15}$$

$$E_{Cl} = 26.64 \ln\left(\frac{[Cl^-]_i}{[Cl^-]_o}\right), \tag{16}$$

$$E_{Ca} = \frac{26.64}{2} \ln\left(\frac{[Ca^{2+}]_o}{[Ca^{2+}]_i}\right). \tag{17}$$

The numerator and denominator in Eq. (16) are reversed to account for the negative charge on chloride ions. The units and description of various parameters used in the model are given in Table 1.

The concentration of each ion type is continuously updated by integrating the relevant ion currents and fluxes as in Wei et al. (2014b). The rate of change of the number of extracellular K^+ ions, $\frac{dNK_o^+}{dt}$, is a function of I_K, I_{pump}, lateral K^+ diffusion (I_{diff}) from/to bath solution *in vitro* or blood vessel *in vivo*, glial uptake surrounding the neurons (I_{glia}) (Cressman et al. 2009), glial Na^+/K^+ pump current ($I_{gliapump}$) (Øyehaug et al. 2012), $Na^+/K^+/Cl^-$ cotransport (I_{nkcc1}), and K^+/Cl^- cotransport (I_{kcc2}) (Payne et al. 2003). The rate of change of the number of intracellular K^+ ions, $\frac{dNK_i^+}{dt}$ is a function of I_K, I_{pump}, I_{nkcc1}, and I_{kcc2}. The rates of change of the number of intracellular $\left(\frac{dNNa_i^+}{dt}\right)$ and extracellular $\left(\frac{dNNa_o^+}{dt}\right)$ Na^+, , are modeled based on I_{Na}, I_{pump}, and I_{nkcc1}. The dynamics of the number of intracellular (NCl_i^-) and extracellular (NCl_i^-) Cl^- ions is a function of I_{Cl}, I_{nkcc1}, and I_{kcc2}. The number of intracellular Ca^{2+} ions ($NCa^{2+}{}_i$) is a function of voltage-gated Ca^{2+} channels in the plasma membrane, the release

Table 1 Values and units of various parameters used in the model

Parameters	Units	Description
C_m	$1\ \mu F/cm^2$	Membrane capacitance
G_{Na}	$30 mS/cm^2$	Maximum conductance of sodium current
G_k	$25 mS/cm^2$	Maximum conductance of potassium current
G_{NaL}	$0.0247 mS/cm^2$	Maximum conductance of leak sodium current
G_{KL}	$0.05 mS/cm^2$	Maximum conductance of leak potassium current
G_{CIL}	$0.1 mS/cm^2$	Maximum conductance of leak chloride current
β_v	5.4	Ratio cytosolic and mitochondria/ER volumes
β_o	7	Initial value of intra-/extracellular volume ratio
ρ_{max}	0.4 mM/s	Maximum Na^+/K^+ pump rate
G_{gmax}	5mM/s	Maximum glial uptake strength of K^+
ϵ_{kmax}	0.25/s	Maximum potassium diffusion rate
$[K^+]_{bath}$	4-40mM	K^+ concentration in the bath
σ	0.1/s	Oxygen diffusion rate
α	5.3 g/mol	Conversion factor from mg/L to mM
$[O_2]_{bath}$	0-32 mg/L	Oxygen concentration in the bath
U_{kcc2}	0.3 mM/s	Maximum strength of KCC2 cotransporters
U_{nkcc1}	0.1 mM/s	Maximum strength of NKCC1 cotransporters
a_2	$0.14/\mu$Ms	Ca^{2+} inhibition constant
d_1	0.005 μM	IP_3R dissociation constant for IP_3
d_2	87.7141 μM	Dissociation constant for Ca^{2+} inhibition IP_3R
d_3	5.3918 nM	IP_3R dissociation constant for IP_3
d_5	0.74 nM	Ca^{2+} activation constant of IP_3R
k_3	0.35 μM	Activation constant for ATP-Ca^{2+} pump
K_e	0.05 μM	Dissociation constant of ATP from SERCA pumps
v_1	18 s^{-1}	Maximum IP_3R channel flux
v_2	0.0408 s^{-1}	Maximum Ca^{2+} leak flux from ER
v_3	4.404 $\mu M^{-1}\ s^{-1}$	Maximum Ca^{2+} uptake by SERCA

The parameters used in mitochondrial model are given in the supplementary information of Toglia et al. (2016)

of Ca^{2+} from mitochondria through Na^+/Ca^{2+}-exchanger (V_{NaCa}), Ca^{2+} uptake by mitochondria through uniporter (V_{uni}), Ca^{2+}-release through inositol 1,4,5-trisphosphate (IP_3) receptors (IP_3Rs) and Ca^{2+} leak channels (V_{ERout}) from the endoplasmic reticulum (ER), and Ca^{2+} uptake by ER through sarco-ER Ca^{2+}-ATPase (serca) activity (V_{SERCA}). The rate equations governing the number of different ion species are:

$$\frac{dNK_o^+}{dt} = \tau\upsilon_o(\beta(\gamma I_K - 2I_{pump} + I_{kcc2} + I_{nkcc1}) - I_{diff} - I_{glia} - 2I_{gliapump}), \quad (18)$$

$$\frac{dNK_i^+}{dt} = \tau\upsilon_i(-\gamma I_K + 2I_{pump} - I_{kcc2} - I_{nkcc1}), \quad (19)$$

$$\frac{dNNa_o^+}{dt} = \tau\upsilon_o\beta(\gamma I_{Na} + 3I_{pump} - I_{nkcc1}), \quad (20)$$

$$\frac{dNNa_i^+}{dt} = \tau\upsilon_i(-\gamma I_{Na} - 3I_{pump} + I_{nkcc1}), \quad (21)$$

$$\frac{dNCl_o^-}{dt} = \tau\upsilon_o\beta(-\gamma I_{ClL} + I_{kcc2} + 2I_{nkcc1}), \quad (22)$$

$$\frac{dNCl_i^-}{dt} = \tau\upsilon_i(\gamma I_{ClL} - I_{kcc2} - 2I_{nkcc1}), \quad (23)$$

$$\frac{dNCa_i^{2+}}{dt} = \tau\upsilon_i\left[\left(\frac{-\gamma G_{ca}(V_m - E_{Ca})}{1+exp(-(V_m+25)/2.5)} - \frac{[Ca^{2+}]_i}{5}\right) + \beta_v(V_{NaCa} - V_{uni} + V_{ERout} - 2V_{serca})\right]. \quad (24)$$

τ = 0.001 is used to convert time from milliseconds to seconds. υ_i, υ_o, G_{Ca}, and $[Ca^{2+}]_i$ represent intracellular volume of the neuron, extracellular volume, maximum conductance of voltage-gated Ca^{2+} channels, and intracellular Ca^{2+} concentration respectively. $\beta = \upsilon_i/\upsilon_o$ and β_v is the relative volume of the ER or mitochondria with respect to the cytoplasm. The factor 2 or 3 in front of I_{pump} indicates the electrogenic ratio of Na^+/K^+ pump, while that in front of I_{nkcc1} indicates that $Na^+/K^+/Cl^-$ cotransporter transports two Cl^- ions with one Na^+ and one K^+ ion. The factor 2 in front of V_{serca} accounts for the two Ca^{2+} ions transferred by SERCA pump from cytoplasm to ER at the expense of one ATP molecule. The term $[Ca^{2+}]_i/5$ in Eq. (24) mimics the absorption of cytosolic Ca^{2+} due to buffers.

The ion concentrations are calculated by dividing the number of ions for a given specie by the volume of the compartment. That is, $[\bullet]_i = N_i/\upsilon_i$, $[\bullet]_o = N_o/\upsilon_o$, where i and o indicate intracellular and extracellular space respectively.

The functional forms of I_{pump}, I_{glia}, and I_{diff} are taken from Cressman et al. (2009) and Wei et al. (2014b) and modified below to incorporate the ATP dependence of these fluxes. For $I_{gliapump}$, we use the same functional form as for the neuronal pump but with 1/3 the strength of neuronal pump. This ratio was used because the relative resting energy consumption in neurons versus glia is ~ 3:1 (Attwell and Laughlin 2001).

$$I_{pump} = \frac{p}{1+\exp(25-[Na^+]_i)/3} \times \frac{1}{1+\exp(3.5-[K^+]_o)}, \quad (25)$$

$$I_{gliapump} = \frac{1}{3}\frac{p}{1+\exp((25-[Na^+]_{gi}))/3} x \frac{1}{1+\exp(3.5-[K^+]_o)}. \quad (26)$$

Where $[Na^+]_{gi}$ is the Na^+ concentration in the glia compartment. We assume a fixed $[Na^+]_{gi}$=18mM (Wei et al. 2014b).

With ATP dynamics included in the model, we have modified the Na^+/K^+ pump rate (p) in Eqs. (25) and (26) to be explicitly dependent on the ATP concentration ([ATP]) produced by mitochondria using a sigmoid function of [ATP] as:

$$p = \frac{\rho}{1+\exp\left(\frac{-[ATP]}{9\times10^{-5}}\right)}, \quad (27)$$

where ρ represents maximum pump strength. Both the neuronal and glial Na^+/K^+-ATP pump strengths decrease as the cell depletes its [ATP] stores.

I_{glia} represents the combined effect of glial K^+ uptake through inward rectified K^+ channels and $Na^+/K^+/Cl^-$ cotransporters.

$$I_{glia} = \frac{G_{glia}}{(1+\exp((18-[K^+]_o)/2.5))}. \quad (28)$$

The diffusion of K^+ between extracellular space and vasculature is modeled as Cressman et al. (2009):

$$I_{diff} = \epsilon_k([K^+]_o - [K^+]_{bath}). \quad (29)$$

ϵ_k and $[K^+]_{bath}$ represent the diffusion coefficient of K^+ and bath K^+ concentration in the bath respectfully.

In the brain, glial cells are in contact with blood vessels and form a substantial component of the blood brain barrier. Ion transport between blood vessels and glial cells is dependent upon active transport through the Na^+/K^+ pumps (Gloor 1997). To simulate HSD, the uptake of K^+ ions by the glial cells (G_{glia}) and diffusion of K^+ to the blood vessels or bath (ϵ_k) were modified such that they depend on oxygen concentration in the bath solution or vasculature ($[O_2]_{bath}$). ϵ_k is also made a function of β to reflect the dependence of K^+ diffusion on the relative

extracellular volume (Syková and Nicholson 2008) (see Wei et al. (2014b) for further details).

$$G_{glia} = \frac{G_{gmax}}{1 + \exp(-([O_2]_{bath} - 2.5)/0.2)}, \quad (30)$$

$$\epsilon_k = \frac{1.0}{1.0 + \exp((-20 + \beta)/2)} \frac{\epsilon_{kmax}}{1 + \exp(-([O_2]_{bath} - 2.5)/0.2)}, \quad (31)$$

where G_{gmax} and ϵ_{kmax} represent maximum glial uptake strength and maximum potassium diffusion coefficient. In fully oxygenated state with normal K^+ in the bath solution, $G_{glia} = G_{gmax}$ and $\epsilon_k = \epsilon_{kmax}$.

The fluxes through NKCC1 and KCC2 cotransporters are modeled in a Nernst-like manner (Wei et al. 2014b):

$$I_{nkcc1} = U_{nkcc1} f([K^+]_o) \left(\ln \left(\frac{[K^+]_i [Cl^-]_i}{[K^+]_o [Cl^-]_o} \right) + \ln \left(\frac{[Na^+]_i [Cl^-]_i}{[Na^+]_o [Cl^-]_o} \right) \right), \quad (32)$$

$$f([K^+]_o) = \frac{1}{1 + \exp(16 - [K^+]_o)}, \quad (33)$$

$$I_{kcc2} = U_{kcc2} \ln \left(\frac{[K^+]_i [Cl^-]_i}{[K^+]_o [Cl^-]_o} \right). \quad (34)$$

Where U_{nkcc1} and U_{kcc2} are cotransporter strengths (Payne et al. 2003; Østby et al. 2009), estimated using the peak conductances given in Lauf and Adragna (2000).

2.2 Oxygen and ATP pumps

Neuronal spiking consumes the most ATP and in turn O_2 in the brain (Lennie 2003). In our model, the oxygen consumption can be estimated by the activity of the neuron and mitochondria where the rate of change in the neuronal ($[O_2]_n$) and mitochondrial ($[O_2]_{mito}$) oxygen concentration depend on the amount present in the bath solution $[O_2]_{bath}$, the mitochondrial oxygen consumption (V_{O2}), and rates of proton pumping due to NADH and $FADH_2$ oxidation denoted by V_{HE} and $V_{HE(f)}$, respectively.

Each proton pump is responsible for the proton ejection from mitochondrion, linked to the transfer of electrons from NADH or $FADH_2$ and is dependent upon proton motive force ($\triangle\mu_H$) and redox potential (A_{res}). The Altman-King-Hill model for a respiration-driven proton pump incorporates a transfer of 2 electrons in the matrix and the ejection of 12 protons by the oxidation of 1 NADH in the inner mitochondrial membrane. Similarly, the model includes the transfer of 2 electrons in the matrix with the ejection of 8 protons by the oxidation of 1 $FADH_2$, while V_{O2} pumps 2 protons per oxidation cycle of NADH and $FADH_2$ (Magnus and Keizer 1997). These stoichiometric relations are incorporated in the rate equation for $[O_2]_{mito}$ as follows.

$$\frac{d[O_2]_{mito}}{dt} = \tau(\sigma([O_2]_n - [O_2]_{mito}) - \alpha(V_{O_2}/2 + V_{HE}/12 + V_{HE(f)}/8)), \quad (35)$$

where the first term represents the transfer of O_2 from neuronal extracellular space to mitochondria and is modeled with a simple diffusion. The diffusion constant, σ is obtained from Fick's law, σ=D/Δx^2. We use a diffusion coefficient D = 1.7 x 10^{-5} cm^2/s for oxygen in brain tissue (Homer et al. 1983) and Δx = 100 μm for the average distance from electrode tip to the surface of the slice or blood vessel to the neuron. α is a conversion factor from mM/sec to $mg/(L \times sec)$ units.

O_2 available to the neuron is simply governed by diffusion from and to the bath solution and mitochondria.

$$\frac{d[O_2]_n}{dt} = \tau\sigma(O_{bath} - 2O_n - O_{mito}), \quad (36)$$

where O_{bath} is the oxygen concentration in the perfusion solution with a normal value of $\sim$ 32 mg/L.

2.3 Volume dynamics

The dynamics of cell volume is modified from the work in Kager et al. (2007) where the instantaneous intracellular volume ($\hat{\upsilon}_i$) depends on the difference between the total extracellular (π_o) and intracellular (π_i) ion concentrations:

$$\hat{\upsilon}_i = \upsilon_i^0(1.1029 - 0.1029\exp((\pi_o - \pi_i)/20)), \quad (37)$$

where υ_i^0 is the initial volume of the cell and

$$\pi_o = [Na^+]_o + [K^+]_o + [Cl^-]_o + [Ca^{2+}]_o + [A^-]_o \quad (38)$$

$$\pi_i = [Na^+]_i + [Cl^-]_i + [K^+]_i + [Ca^{2+}]_i + [A^-]_i. \quad (39)$$

$[A^-]_i$ = 132 mM and $[A^-]_o$ = 18 mM are the intra- and extracellular concentration of impermeable anions, calculated by assuming that the initial osmotic pressure gradient is zero (Wei et al. 2014b). We implement the change of volume as a first-order process with a time-constant of 250 ms (Kager et al. 2007):

$$\frac{dVol_i}{dt} = \tau\frac{(\hat{\upsilon}_i - \upsilon_i)}{250} \quad (40)$$

2.4 Ca^{2+} dynamics in endoplasmic reticulum

To simulate Ca^{2+} concentration in the ER ($[Ca^{2+}]_{ER}$), we use our previously developed model (Ullah et al. 2006), where Ca^{2+} is released through IP_3R and leak channels and pumped back through SERCA, i.e.

$$\frac{d[Ca^{2+}]_{ER}}{dt} = \tau(2V_{serca} - V_{ERout}), \quad (41)$$

where the factor 2 in front of V_{serca} accounts for the two Ca^{2+} ions transferred by SERCA pump from cytoplasm to ER at the expense of one ATP molecule.

The SERCA pump is modified to include dependence on ATP produced by the mitochondria (Wacquier et al. 2016).

$$V_{serca} = v_3 \left(\frac{[Ca^{2+}]_i^{\,2}}{k_3^2 + [Ca^{2+}]_i^{\,2}} \right) \left(\frac{[ATP]}{K_e + [ATP]} \right). \tag{42}$$

V_{ERout} is a combination of Ca^{2+} flux through IP_3R and the leak channels.

$$V_{ERout} = (v_1 P_o + v_2)([Ca^{2+}]_{ER} - [Ca^{2+}]_i), \tag{43}$$

where P_o is the open probability of IP_3R. The gating of IP_3R is modeled with a simple two-state model where the receptor is assumed to have four subunits and is open when at least three of the four subunits are in open state. Each subunit can be in a closed (c) or active (h_{er}) state (Li and Rinzel 1994).

$$c \underset{\beta_{er}}{\overset{\alpha_{er}}{\rightleftharpoons}} h_{er}. \tag{44}$$

Where $\alpha_{er} = a_2 Q_2$, $\beta_{er} = a_2[Ca^{2+}]_i$, and

$$Q_2 = \frac{d_2(IP_3 + d_1)}{IP_3 + d_3}. \tag{45}$$

The fraction of subunits in active state is given as

$$\frac{dh_{er}}{dt} = \alpha_{er}(1 - h_{er}) - \beta_{er} h_{er}. \tag{46}$$

At steady-state, the open-probability of IP_3R channels is

$$P_o = \left(\frac{[IP_3]}{[IP_3] + d_1} \right)^3 \left(\frac{[Ca^{2+}]_i}{[Ca^{2+}]_i + d_5} \right)^3 h_{\infty er}^3, \tag{47}$$

where

$$h_{\infty er} = \frac{\alpha_{er}}{\alpha_{er} + \beta_{er}}. \tag{48}$$

Where $[IP_3] = 50nM$ is the concentration of $IP_3R's$ ligand, IP_3.

2.5 Mitochondrial dynamics

The rate equations modeling mitochondrial function are listed in Table 2S. Full details of these equations and various fluxes involved are given in Supplementary Information Text and (Toglia et al. 2016). Here, we present the three fluxes that are modified from Toglia et al. (2016) to incorporate their dependence on the dynamics of $[O_2]_{mito}$. These fluxes are oxygen consumption flux (V_{o_2}) and the two linked proton effluxes (V_{HE} and $V_{HE(f)}$) that also depend on $\Delta\mu_H$ and A_{res}.

$$V_{HE} = V_{Hemax} \left(\frac{O_{mito}}{K_o + O_{mito}} \right) \frac{r_a e^{\frac{A_{res}F}{RT}} - (r_a + r_b)\, e^{\left(\frac{gF\Delta\mu_H}{RT}\right)}}{\left(1 + r_1 e^{\left(\frac{FA_{res}}{RT}\right)}\right) e^{\left(\frac{6F\Delta\Psi_B}{RT}\right)} + \left(r_2 + r_3 e^{\left(\frac{FA_{res}}{RT}\right)}\right) e^{\left(\frac{g6F\Delta\mu_H}{RT}\right)}} \tag{49}$$

$$V_{He(f)} = V_{He(f)max} \left(\frac{O_{mito}}{K_o + O_{mito}} \right) \frac{r_a e^{\frac{A_{res(f)}F}{RT}} - (r_a + r_b)\, e^{\left(\frac{gF\Delta\mu_H}{RT}\right)}}{\left(1 + r_1 e^{\left(\frac{FA_{res(f)}}{RT}\right)}\right) e^{\left(\frac{6F\Delta\Psi_B}{RT}\right)} + \left(r_2 + r_3 e^{\left(\frac{FA_{res(f)}}{RT}\right)}\right) e^{\left(\frac{g6F\Delta\mu_H}{RT}\right)}} \tag{50}$$

$$V_{o_2} = V_{O_2max} \left(\frac{O_{mito}}{K_o + O_{mito}} \right) \frac{\left(r_a + r_{c1} e^{\left(\frac{6F\Delta\Psi_B}{RT}\right)}\right) e^{\left(\frac{A_{res}F}{RT}\right)} - r_a e^{\left(\frac{g6F\Delta\mu_H}{RT}\right)} + r_{c2} e^{\left(\frac{A_{res}F}{RT}\right)} e^{\left(\frac{gF\Delta\mu_H}{RT}\right)}}{\left(1 + r_1 e^{\left(\frac{FA_{res}}{RT}\right)}\right) e^{\left(\frac{6F\Delta\Psi_B}{RT}\right)} + \left(r_2 + r_3 e^{\left(\frac{FA_{res}}{RT}\right)}\right) e^{\left(\frac{g6F\Delta\mu_H}{RT}\right)}} \tag{51}$$

Since different pumps consume ATP produced by the mitochondria, the functional form of [ATP] is now:

$$[ATP] = C_m - [ADP] - (I_{gliapump} + I_{pump} + V_{serca})dt \tag{52}$$

where [ADP] is the concentration of adenosine diphosphate, C_m is the total sum of mitochondria's adenine nucleotides, and dt is the time step used in the simulations. Since the adenine nucleotide pool available to mitochondria is known to deplete during SD (Schild et al. 1999), we use the following functional form for C_m, which is coupled to phosphorylation that in turn depends on $\Delta\Psi_m$.

$$C_m = \frac{6.6}{1 + \exp(-(\Delta\Psi_m - 100))} + 8.4 \tag{53}$$

Numerical integration of the full model equations (Tables 1S and 2S) was performed with Intel Fortran compiler (Intel Corporation, Santa Clara, CA). ODEs were solved using RK4 method. Code producing key results in the paper is available upon request from authors.

3 Results

Since our model for neuronal dynamics is capable of reproducing a range of behaviors (see Wei et al. (2014b) for details), the full mathematical framework developed here can be used to investigate mitochondrial behavior in all those behaviors. Here we focus on SZ, SD, and HSD.

3.1 Neuronal dynamics during SZ, SD, and HSD

Figure 2 illustrates typical neuronal membrane potential and $[K^+]_o$ traces during HSD, SZ, and SD where one can see the typical neuronal behavior during these conditions. In line with observed neuronal behavior (Czéh et al. 1993), severe hypoxia leads to a single-episode of SD, where the membrane potential of the cell is locked into a depolarized state and $[K^+]_o$ reaches near 50 mM. The neuronal membrane depolarizes because the lack of oxygen leads to a sudden drop in cellular ATP levels, and consequently impaired function of ATP-dependent pumps that fail to maintain ion gradients across the plasma membrane. Other ions go through major changes in a similar fashion (not shown) that can only recover after normal oxygen supply is restored (Fig. 2a and b). Elevating $[K^+]_{bath}$ to 8 mM under normal $[O_2]_{bath}$, the cell exhibits rapid periodic spiking that are characteristic of seizures (Fig. 2c and d). Increasing $[K^+]_{bath}$ further leads to SD (Fig. 2e and f). The initial spiking during SD is consistent with single-cell recordings observed experimentally (Brisson and Andrew 2012; Hosseini-Zare et al. 2017; Hübel et al. 2017). Due to osmotic imbalance in the neuron, we observe significant neuronal swelling during HSD, SZ, and SD, leading to increased ratio of intracellular to extracellular volume (Fig. 1S).

We previously showed that SZ, SD, and HSD lie along a continuum where one can observe these three and several other neuronal behaviors by only varying $[K^+]_{bath}$ and/or $[O_2]_{bath}$ (Ullah et al. 2015; Wei et al. 2014b). Specifically, at lower $[K^+]_{bath}$, the neuron exhibits normal behavior with regular spiking in response to applied stimulus (Wei et al. 2014b). As we increase $[K^+]_{bath}$ beyond 8 mM (from a normal value of 3-4 mM), the cell exhibits SZ-like spiking. SD on the other hand, is observed when $[K^+]_{bath}$ exceeds 12 mM. A recent experimental study confirmed these predictions *in vivo* in multiple animal models of epilepsy by showing that single seizures are frequently associated with SD, and that SD may mediate between seizures within clusters (Bahari et al. 2018). These findings lend strong support to the proposal that seizure-triggered SD could underlie sudden unexplained death in epilepsy (Aiba and Noebels 2015). The synergy between SZ and SD have also been reported in experimental models of acute hyperexcitability including low-magnesium (Avoli et al. 1991; Mody et al. 1987) and high K^+ (Gabriel et al. 2004)

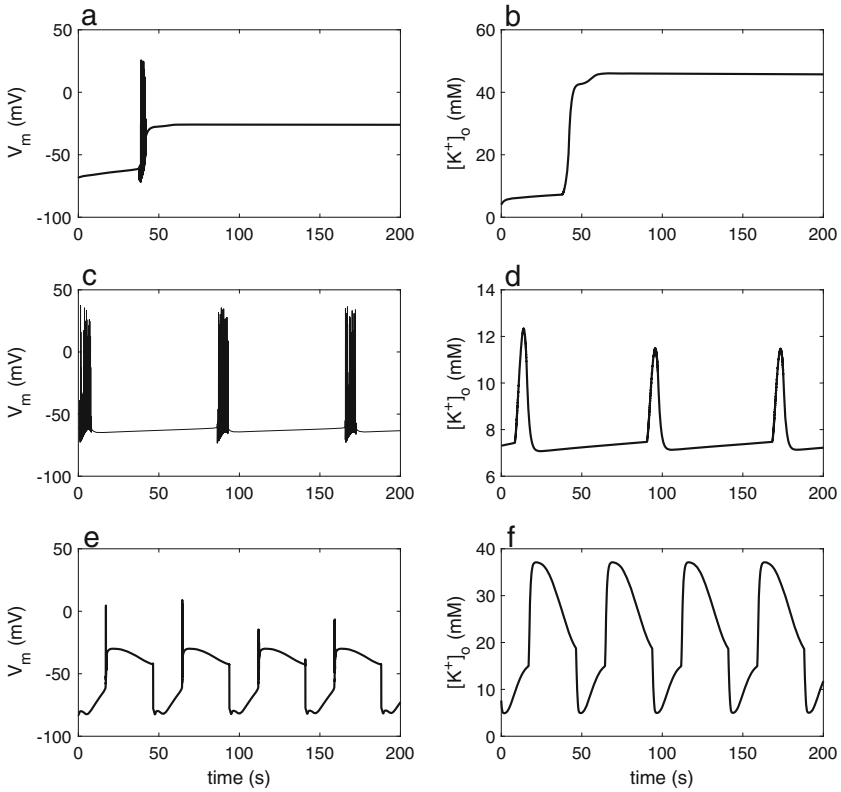

Fig. 2 Membrane potential (V_m) and $[K^+]_o$ during HSD, SZ, and SD. Membrane potential **a** and $[K^+]_o$ **b** during HSD where $[K^+]_{bath}$ = 4mM and $[O_2]_{bath} \sim 0$ mg/L. Membrane potential **c** and $[K^+]_o$ **d** during SZ where $[K^+]_{bath}$ = 8mM and $[O_2]_{bath}$ = 32 mg/L. Membrane potential **e** and $[K^+]_o$ **f** during SD where $[K^+]_{bath}$ = 40mM and $[O_2]_{bath}$ = 32 mg/L

in rodent and human brain slices, models of disinhibition (Hablitz and Heinemann 1989; Köhling et al. 2003), Na^+/K^+ pump inhibition (Major et al. 2017; Vaillend et al. 2002), and electrical stimulation in hippocampal slices (Pomper et al. 2006). The transition between SZ and SD is also important for the amount of Gibbs free energy possessed by the cell that it can use to perform work and maintain the ion gradients across its plasma membrane and membranes of intracellular organelles. The loss in Gibbs free energy during SD is almost ten times higher than that in SZ, leaving the cell more vulnerable to cytotoxic edema (Dreier et al. 2013). More importantly, the co-occurrence of ictal epileptiform events and SDs was recently reported in patients with aneurysmal subarachnoid hemorrhage, spontaneous intracerebral hemorrhage and traumatic brain injury (Dreier et al. 2011; Fabricius et al. 2008). Such unification of various neuronal behaviors is maintained by the model even after incorporating the mitochondrial function as demonstrated by the bifurcation diagram showing the minimum and maximum of $[K^+]_o$ as we vary $[K^+]_{bath}$ (Fig. 3). The steady state $[K^+]_o$ at $[K^+]_{bath} < 8mM$ indicates the absence of of spontaneous spiking, whereas the low amplitude oscillations in the range $8mM < [K^+]_{bath} < 12mM$ indicate spontaneous seizures as shown in Fig. 2c. The large amplitude oscillations in $[K^+]_o$ at $[K^+]_{bath} > 12mM$ on the other hand are reminiscent of spontaneous periodic SDs (Fig. 2e). Later, we will show how different variables governing mitochondrial function can affect this bifurcation and other aspects of SZ and SD.

3.2 Mitochondrial function during HSD, SZ, and SD

Due to large depolarization of neuronal membrane during HSD, SZ, and SD, Ca^{2+} influx into the neuron can disrupt the normally tightly regulated Ca^{2+} dynamics, resulting in dramatic rise in intracellular Ca^{2+} concentration (Bahar et al. 2000). Furthermore, significant increase in glutamate due to excessive neuronal spiking (Hübel et al. 2017) leads to the generation of IP_3 that stimulates Ca^{2+} release from intracellular stores through IP_3R, increasing $[Ca^{2+}]_i$ further (Ullah et al. 2006; Zhang and Lipton 1999). Much of the Ca^{2+} that enters cytoplasm either from extracellular space or intracellular compartments is buffered by Ca^{2+} binding proteins and mitochondria. Mitochondrial buffering of excessive $[Ca^{2+}]_i$ can lead to diminished $\Delta\Psi_m$ and [ATP], along with increased reactive oxygen species ($[O_2^-]_m$ and $[H_2O_2]$) (Toglia et al. 2016). As organelles of oxidative metabolism, mitochondria are especially susceptible and critically involved in HSD due to low $[O_2]$ availability. Fig. 4a and b illustrate how large amount of Ca^{2+} enters the cytoplasm due to cell's membrane depolarization during HSD and $[Ca^{2+}]_m$ consistently rises as mitochondria buffers the large influx of Ca^{2+}. The rapid depolarization of $\Delta\Psi_m$ (Fig. 4c) and influx of Ca^{2+} into the matrix coupled with no O_2 availability for NADH (Fig. 4d and $FADH_2$ oxidation, leads to diminished proton pumping and subsequently a rapid drop in ATP production (Fig. 4e). Although $\Delta\Psi_m$ and ATP are diminished, NADH saturates because of the Ca^{2+} influx to the mitochondrial matrix driving TCA cycle enzymes (Fig. 4d). NADH accumulation has been observed

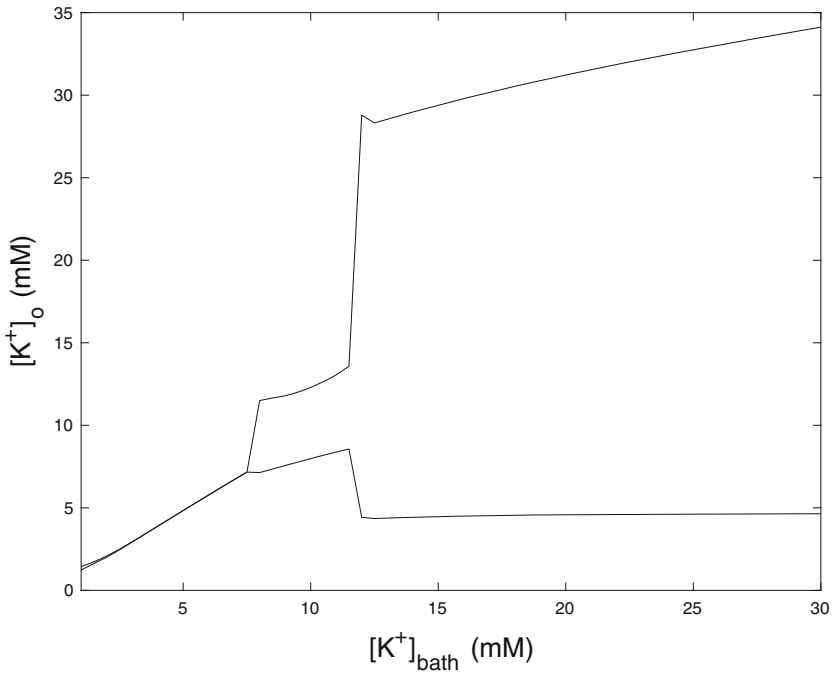

Fig. 3 Bifurcation diagram showing the minimum and maximum of $[K^+]_o$ as a function of $[K^+]_{bath}$ at normal ΔpH=-0.6 and $[P_i]$=20 mM

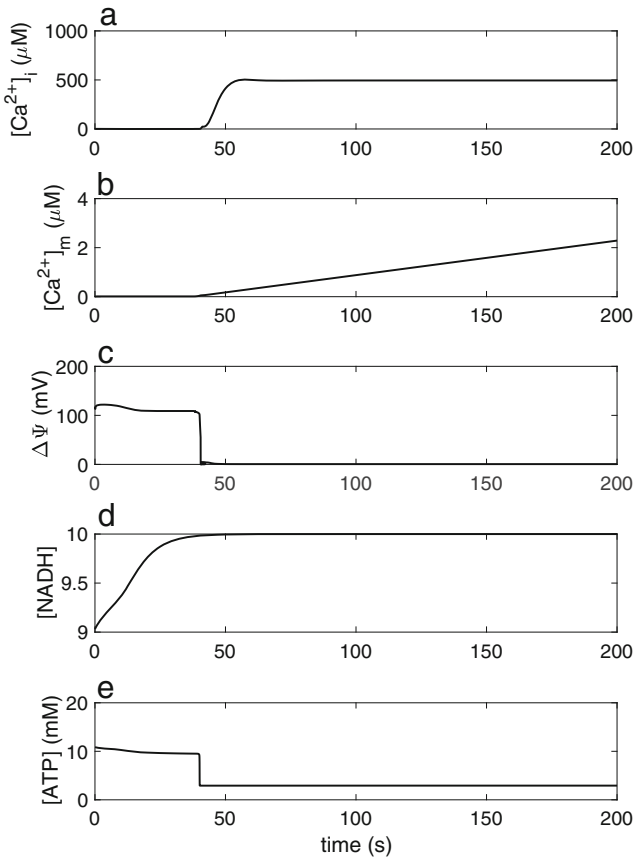

Fig. 4 Changes in mitochondrial variables due to high $[Ca^{2+}]_i$ and low O_2 during HSD. Increased $[Ca^{2+}]_i$ **a** and subsequent mitochondrial Ca^{2+} buffering $[Ca^{2+}]_m$ **b** lead to diminished $\Delta\Psi_m$ **c**, NADH saturation (due to lack of O_2) **d**, and diminished ATP **e** during simulated HSD. HSD was induced in the model by inducing hypoxic conditions in the model, that is by reducing oxygen in the bath solution ($[O_2]_{bath}$) to ~ 0 mg/L at physiological K^+ concentration in the bath ($[K^+]_{bath}$ = 4mM)

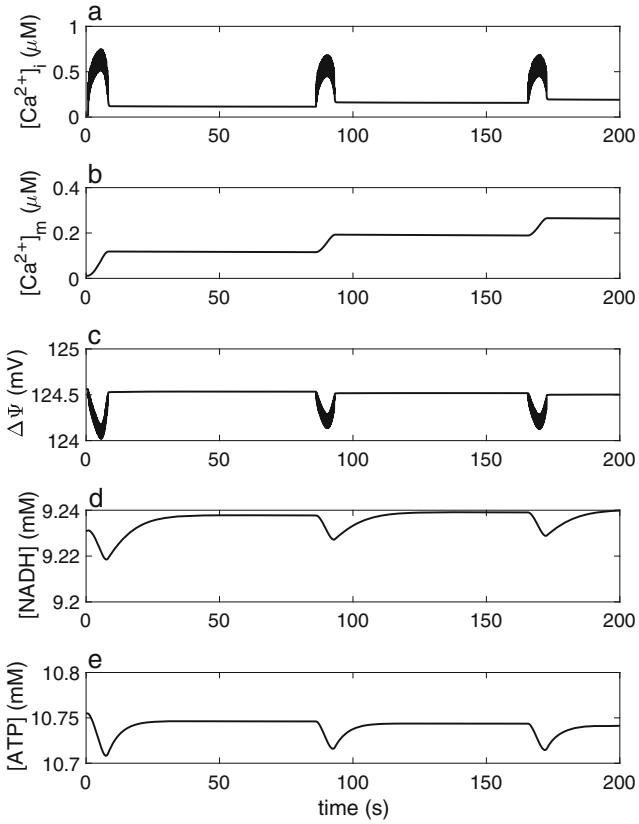

Fig. 5 Changes in mitochondrial variables during SZ. Both $[Ca^{2+}]_i$ **a** and $[Ca^{2+}]_m$ **b** increase during SZ, leading to lower $\Delta\Psi_m$ **c**, [NADH] **d**, and [ATP] **e** during seizures. Seizures were induced by raising K^+ in the bath ($[K^+]_{bath}$) to 8mM at normal oxygen in the model ($[O_2]_{bath}$ = 32 mg/L)

experimentally when O_2 supply is limited (Mayevsky et al. 1982; Rosenthal and Martel 1979; Schechter et al. 2009). Diminished $\Delta\Psi_m$ and ATP shown in our model due to HSD are also consistent with experimental observations (Lothman et al. 1975; Bahar et al. 2000; Somjen 2001).

Intracellular Ca^{2+} also increases significantly during periodic seizures (Fig. 5a), leading to increased $[Ca^{2+}]_m$ (Fig. 5b). The increase in $[Ca^{2+}]_m$ looks much like increasing periodic steps due to the relatively high-frequency of $[Ca^{2+}]_i$ oscillations and mitochondria's inability to efflux enough Ca^{2+} through Na^+/Ca^{2+}-exchanger from the matrix before the next spike of Ca^{2+} due to next seizure occurs. In *in vivo* conditions where the frequency of SZ occurrence is typically lower even when seizures occur in clusters (see for example Bahari et al. (2018)), Na^+/Ca^{2+} exchangers would have significantly longer time to restore $[Ca^{2+}]_m$. This would lead to the decaying of $[Ca^{2+}]_m$ back to its base level after the seizure is over. Nevertheless, the transient drops in $\Delta\Psi_m$, NADH, and ATP will persist as can be been seen in Fig 5c, d, and e. During Ca^{2+} oscillations, $\Delta\Psi_m$ slightly depolarizes (Fig. 5c) leading to lower NADH and ATP during neuronal spiking (Fig. 5d and e).

Due to stronger depolarization of the cell membrane during SD as compared to SZ (Fig. 2), Ca^{2+} influx into the cytoplasm is much higher (Fig. 6a). This leads to larger Ca^{2+} buffering by mitochondria as compared to SZ-like conditions (Fig. 6b). In seizures, $\Delta\Psi_m$ only decreases by $\sim$ 1 mV whereas in SD, we see close to 4 mV drop in $\Delta\Psi_m$ (Fig. 6c). This exaggerated depolarization of mitochondrial membrane leads to $\sim 50\ \mu$M decrease in NADH and $\sim 200\ \mu$M decrease in ATP (Fig. 6d and e). We believe that with repeated seizures or SD over time, the stress experienced by mitochondria can be detrimental to the neuron's overall ability to function properly. Our observations about the effect of periodic SD on mitochondria are consistent with experimental observations (Kovács et al. 2005; Zhou et al. 2010).

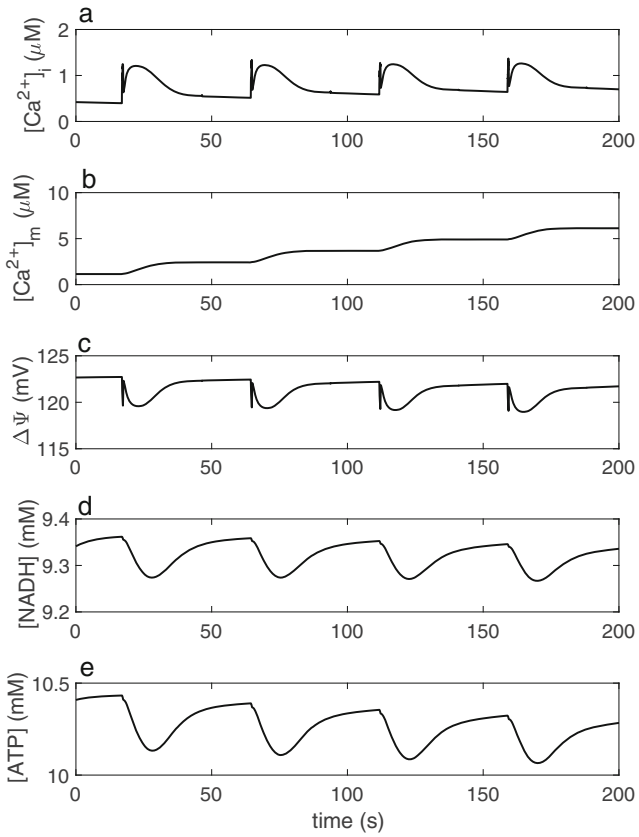

Fig. 6 Changes in mitochondrial variables are more extreme during SD when compared to SZ. Higher $[Ca^{2+}]_i$ **a** and subsequently higher mitochondrial Ca^{2+} buffering **b**, leads to larger decrease in $\Delta\Psi_m$ **c**, [NADH] **d** and [ATP] (E) during SD

3.3 Mitochondrial ability to restore neuronal pumps and recovery

The availability of substrate [ADP] and phosphate ($[P_i]$) are the major contributors to mitochondria's ability to produce ATP. Phosphate directly affects the potential (A_{F1}) of the F_1F_0- ATP synthase. Thus, decreasing $[P_i]$ available to mitochondria diminishes its potential for F_1F_0- ATP synthase to produce [ATP] at its optimal rate for cellular needs. In our model, Na^+/K^+ pumps on neuronal plasma membrane and glia are both dependent on [ATP]. Similarly, SERCA pumps in the ER are also fueled by ATP. All these pumps are responsible for restoring ion gradients to help the neuron recover from SZ or SD. Thus, it is important to understand the effect of mitochondrial $[P_i]$ availability on overall neuronal function.

To evaluate the effect of $[P_i]$ on neuronal function, we simulate the model under HSD ($[O_2]_{bath} \sim 0$ mg/L, all other parameters as given in Table 1) and SD ($[K^+]_{bath}$ = 40mM all other parameters as given in Table 1) for initial 250 sec, followed by restoration of $[O_2]_{bath}$ in HSD and $[K^+]_{bath}$ in SD to normal values for the rest of simulations (Fig. 2S). While neurons recover from HSD only when normal oxygen supply and consequently normal cellular ATP levels are restored in most cases (Hansen 1984; Lipton 1999; Wang et al. 2000), Fig. 2S shows that having higher $[P_i]$ helps to restore ion pumps quicker and subsequently helps the neuron recovers faster from HSD. Figure 2S shows time-traces for V_m (A), I_{pump}(B), and $I_{gliapump}$ (C) at $[P_i]$=5, 10, and 15 mM. Fig. 2SA also indicates that the latency of HSD onset is proportional to $[P_i]$ available to mitochondria. This can be easily seen in Fig. 7a where the latency to HSD onset is shown as a function of $[P_i]$. The amplitude of the depolarization block (the peak membrane potential during HSD or SD) is inversely proportional to $[P_i]$ (Fig. 7b). We also observe that the time for the neuron to make a recovery after $[O_2]_{bath}$ is restored is shorter when larger amount of $[P_i]$ is available to mitochondria (Fig. 7c). Fig. 2Sb and c show that the pumps are more efficient with increasing $[P_i]$ both at onset and recovery, leading to slower onset and faster recovery. More $[P_i]$ availability reduces the drop in ATP during depolarization block and increases the amount of ATP available for recovery (Fig. 7c). Thus, the weakening of ion pumps due to lower $[P_i]$ leads to higher neuronal excitability. As a result, the neuron makes faster transition to HSD from resting state at lower $[P_i]$. Experiencing longer and stronger depolarizations would leave the neuron more vulnerable to injury and irreversible damage (Andrew et al. 2017).

In a similar set of experiments as in Fig. 2S, we change the ΔpH of the mitochondria and evaluate its effect on

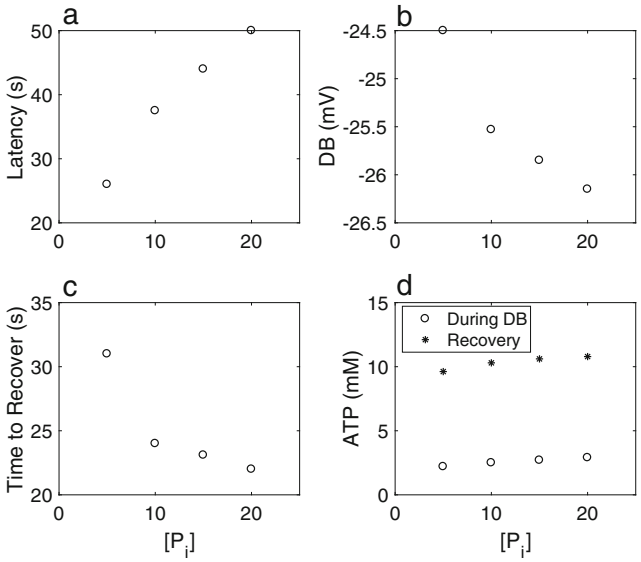

Fig. 7 Higher $[P_i]$ availability weakens HSD. Latency of HSD onset **a**, strength of DB **b**, and time to recover from SD after O_2 is restored **c** as we decrease $[P_i]$ from 20 mM (normal) to 15 mM , 10 mM, and 5 mM. **d** Higher $[P_i]$ leads to slightly higher [ATP] during DB (circles) and after recovery (*), resulting in slow transition to SD and faster recovery of neuron to resting state

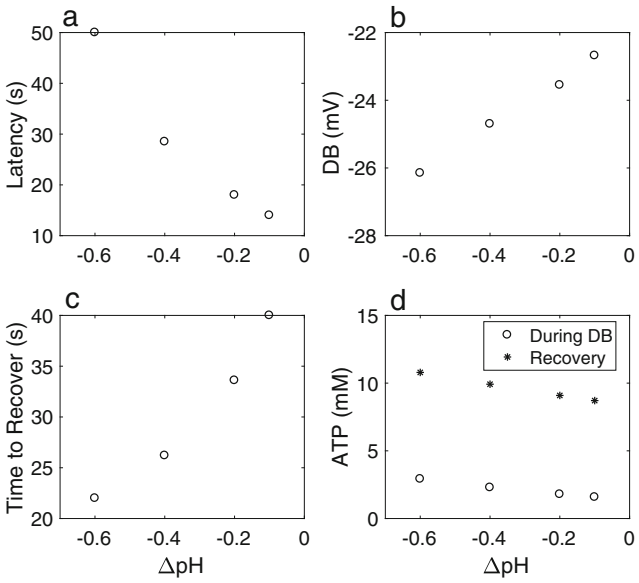

Fig. 8 More negative ΔpH results in weaker HSD. Latency of HSD onset **a**, DB **b**, time to recover from SD after O_2 is restored **c** as we increase ΔpH from -0.6 (normal), to -0.4, -0.2, and -0.1. **d** Lower ΔpH leads to larger [ATP] during DB (circles) and after recovery (*), resulting in slow transition to SD and faster recovery of neuron to resting state

HSD and SD. This corresponds to increasing the pH in the mitochondrial matrix while keeping intracellular pH constant at 7.2. Thus, at normal ΔpH, cytoplasmic pH is 7.2 with mitochondrial pH at 7.8, leading to ΔpH of -0.6 (Magnus and Keizer 1997). The proton motive force ($\Delta\mu_{\mathrm{H}}$) is dependent on ΔpH and a stronger pH gradient allows for a stronger $\Delta\mu_{\mathrm{H}}$ to pump protons out of mitochondria, leading to higher production of ATP through $\mathrm{F_1F_0}-$ ATP synthase. Latency of the neuron to enter HSD is inversely proportional to ΔpH (Fig. 8a). The depolarization block is also weaker at more negative ΔpH values which leads to faster recovery (Fig. 8b and c). This is again due to the higher ATP levels during depolarization block and after $[\mathrm{O_2}]_{\mathrm{bath}}$ recovery (Fig. 8d) which restores the activity of ATP-dependent pumps rapidly.

Another key observation is the disappearance of seizure state from the bifurcation diagram shown in (Fig. 3) at low $[P_i]$. One can observe the slow merger of SZ and SD states as $[P_i]$ is lowered to $[P_i]$=15 mM (black), $[P_i]$=10 mM (blue), and eventually $[P_i]$=5 mM (red) (Fig. 9a) as compared to the normal $[P_i]$=20 mM (Fig. 3c). A similar disappearance of SZ state can also be observed as ΔpH is increased (Fig. 9b) as compared to normal value (Fig. 3c).

Pathological uptake of Ca^{2+} by mitochondria has a similar effect on SZ, SD, and HSD (Fig. 10). Although not as dramatic as organic phosphate and pH gradients, pathologically higher mitochondrial Ca^{2+} uptake through uniporter lowers the $[K^+]_{bath}$ threshold at which the neuron makes transition from SZ to SD (Fig. 10a), shortens the latency from the time at which $[O_2]_{bath}$ is set to zero to the instant at which the cell enters HSD (Fig. 10b), and elongates the recovery time of the neurons from HSD after $[O_2]_{bath}$ is restored to normal value (Fig. 10c).

4 Discussion

In this study, we couple the model reproducing neuronal behavior during several conditions including SZ, SD, and HSD (Wei et al. 2014b) with a model for mitochondria function (Toglia et al. 2016), incorporating oxidative phosphorylation, tricarboxylic acid (TCA) cycle, and Ca^{2+} dynamics in mitochondria, cytoplasm, and the ER. This allowed us to incorporate the ATP-dependence of $Na^+/K^+ - ATPase$ in the neuronal and glia plasma

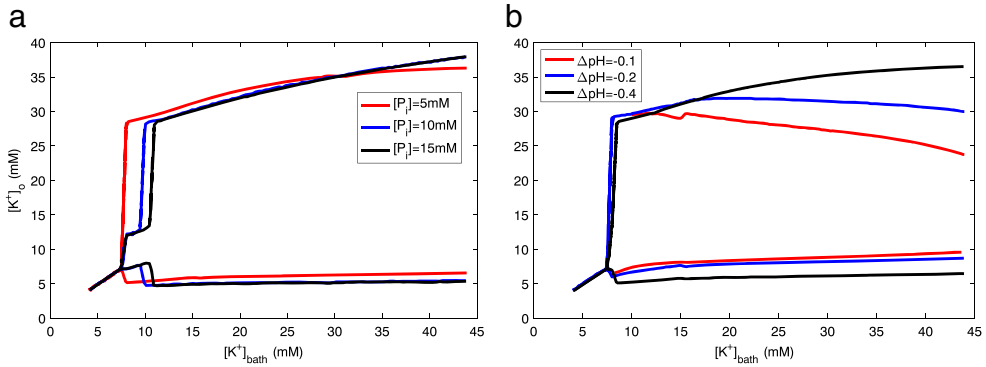

Fig. 9 The SZ state disappears from bifurcation diagram at low $[\mathrm{P_i}]$ and higher ΔpH, resulting in higher neuronal excitability. **a** Minimum and maximum of $[K^+]_o$ as a function of $[K^+]_{bath}$ at $[P_i]$=5 mM (Red), $[P_i]$=10 mM (Blue), and $[P_i]$= 15 mM (black). **b** Minimum and maximum of $[K^+]_o$ at ΔpH= -0.1 (red), -0.2 (blue), and -0.4 (black). Note the fusion between SZ and SD states as $[P_i]$ availability decreases and ΔpH increases as compared to their normal values used in Fig. 3c

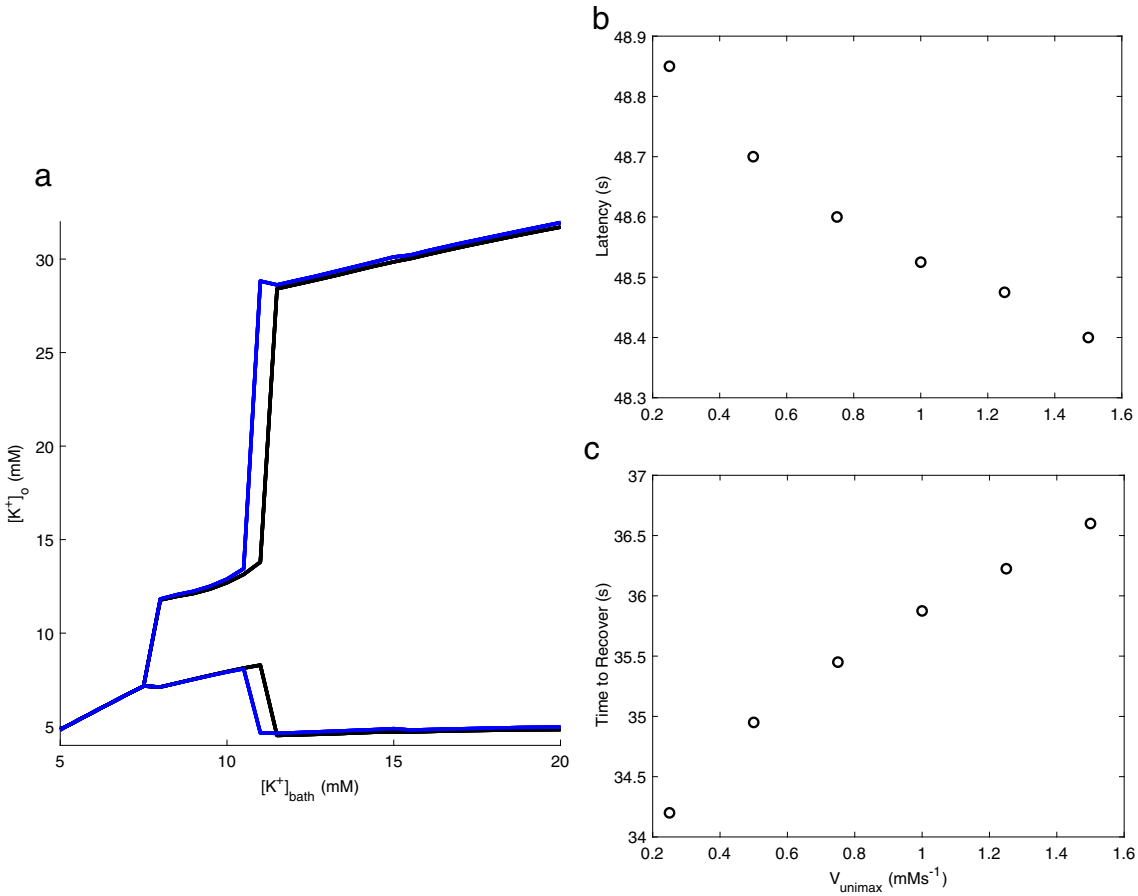

Fig. 10 Higher mitochondrial Ca^{2+} uptake leads to higher excitability that worsens neuronal behavior during SZ, SD, and HSD. **a** Minimum and maximum of $[K^+]_o$ as a function of $[K^+]_{bath}$ at normal ($V_{unimax} = 6.25mMs^{-1}$, black) and 15 times higher (blue) mitochondrial Ca^{2+} uptake through MCU. Latency of HSD onset (**a**) and time to recover from SD after normal O_2 supply is restored **b** as we change maximum mitochondrial Ca^{2+} flux through MCU relative to normal value ($V_{unimax} = 6.25mMs^{-1}$)

membranes, and SERCA pumps on the ER into the model. Using this comprehensive framework, one can not only evaluate the effect of a broad range of pathological neuronal behaviors on mitochondrial dynamics, but can also determine the feedback of impaired mitochondrial function into the dynamics of these phenomena.

Predictions from our model are largely in line with experimental results. Fluorescence imaging using rhodamine-123 of mitochondrial signals in CA1 and CA3 region of rat hippocampus during SZ, SD, and HSD implicates diminished $\triangle\Psi_m$ (Bahar et al. 2000; Kovács et al. 2005), leading to lower $\triangle\mu_H$. These observations are consistent with Figs. 4, 5, and 6 where HSD, SZ, and SD all lead to diminished $\triangle\Psi_m$ and ATP. Furthermore, high cytoplasmic Ca^{2+} during SZ, SD, and HSD was shown to drastically increase $[Ca^{2+}]_m$, and reduce ATP synthesis as a result of Ca^{2+}-dependent activation of mitochondrial dehydrogenases (Kovács et al. 2005). Decreased [NADH] during SZ (Kovács et al. 2002) and SD (Sonn and Mayevsky 2000) has been observed in the presence of normal O_2, consistent with our observations in Figs. 5 and 6. Conversely, increased NADH has been observed when O_2 supply is limited (Mayevsky et al. 1982; Rosenthal and Martel 1979; Schechter et al. 2009), consistent with our observations in Fig. 4.

HSD is shown to be most detrimental to mitochondria's ability to produce ATP due to the lack of O_2 and Ca^{2+} overload. During hypoxia, mitochondria undergoes initial depolarization that appears to be caused by reduced electron transport due to the lack of O_2 (Kovács et al. 2005). In our mitochondrial model, efflux of protons from oxidation of NADH and $FADH_2$ is directly dependent upon $[O_2]_{mito}$. While Ca^{2+} load in mitochondria is not necessary to cause mitochondrial dysfunction in HSD, influx of Ca^{2+} has been shown experimentally to accelerate cell damage (Nicholls and Budd 2000; Scanlon et al. 2000; Kovács et al. 2005).

$[Ca^{2+}]_m$ accumulation can also lead to the opening of permeability transition pore (PTP) into high conductance state, a key mechanism for mitochondrial dysfunction and apoptosis (Friberg and Wieloch 2002; Toglia and Ullah 2016). Blockade of PTP by inhibitor cyclosporin-A and NIM811 has been tested on whether mitochondrial depolarization during epileptiform activity was attributable to Ca^{2+}-dependent opening of the PTP (Waldmeier et al. 2002; Kovács et al. 2005). It was shown that fluorescent measurements representing $\Delta\Psi_m$ was not affected by inhibition of PTP (Kovács et al. 2005), but it may modulate the generic feature of SD and its impact on cerebral vasculature where mitochondrial function was rescued with the inhibition (Friberg and Wieloch 2002; Piilgaard et al. 2011). In HSD, $[Ca^{2+}]_m$ continues to rise indicating that $[Ca^{2+}]_m$ levels will cause the transition of PTP to high conductance state as is shown in highly Ca^{2+}-sensitive mitochondria (Hazelton et al. 2009).

In addition to causing diminished $\Delta\Psi_m$, lower ATP, and potentially leading to the opening of PTP, exaggerated mitochondrial Ca^{2+} may also accelerate neuronal damage due to enhanced production and accumulation of $[O_2^-]_m$ and $[H_2O_2]$ as a result of increased oxidative phosphorylation, which are major factors in brain damage (Dreier et al. 1998). Accumulation of $[O_2^-]_m$ and $[H_2O_2]$ has been shown experimentally in SD (Grinberg et al. 2012; Grinberg et al. 2013). Thus, quicker recovery from SZ and SD is important for avoiding accumulation of ROS.

The ability of the neuron to recover from hypoxia faster is crucial in avoiding longterm brain damage. We find that $[P_i]$ and ΔpH both play a key role in helping the neuron recover faster from HSD once O_2 supply is restored (Figs. 7 and 8). In SD, we find that $[P_i]$ and ΔpH help keep the neuron in a polarized state for longer periods of time and the frequency of SD is lower (data not shown), which could minimize neuronal damage. Optimal concentration of $[P_i]$ =20mM and ΔpH=-0.6 bring ATP levels back to steady-state values quicker so that ATP-dependent pumps can recover ionic gradients necessary for normal cell function.

Mitochondria represent an important drug target for many prevalent diseases (Murphy and Hartley 2018; Camara et al. 2010; Bayeva et al. 2013; Jitschin et al. 2014) including stroke (Russo et al. 2018; Liu et al. 2018). While the development of therapies targeting mitochondria was largely focused on diseases caused by mutations in mitochondrial DNA or in nuclear genes encoding mitochondrial proteins, several strategies focusing on mitochondrial function are emerging recently (Murphy and Hartley 2018). Among others, oxidative phosphorylation is one of the primary targets for these emerging therapies. In our model, $[P_i]$ and ΔpH affect SZ, SD, and HSD through mitochondrial F_1F_0- ATP synthase. As expected, increasing $[P_i]$ or ΔpH (more negative) have beneficial effect in these conditions by delaying the onset and decreasing recovery time of HSD. By reducing the cell's excitability, increasing $[P_i]$ or ΔpH also makes the transition from SZ to SD harder (data not shown).

Both $[P_i]$ or ΔpH change significantly during SZ, SD, and HSD. For example, creatine phosphate decreases by up to 80% during spreading depolarization (for example see Ayata and Lauritzen (2015), Gault et al. (1994), Hartings et al. (2017), and Somjen (2004)). Similarly, significant changes in mitochondrial, cytosolic, and extracellular pH occur during anoxia, SD, and HSD (Andersson et al. 1987; Hawrysh and Buck 2019; Ayata and Lauritzen 2015; Hartings et al. 2017; Somjen 2004). Furthermore, both $[P_i]$ and ΔpH offer viable therapeutic targets for these and other conditions. For example, [5-(2-methoxy-5-chloro-5-phenyl)furan-2-ylcarbonyl]guanidine was shown to possess cardioprotective effects in rat hearts during global ischemia by inhibiting Na^+/H^+-exchanger and preserving high-energy phosphates (Lee et al. 2005; Camara et al. 2010; Aldakkak et al. 2008). Blocking Na^+/H^+-exchanger or other channels can also be used to manipulate ΔpH or the proton motive force across mitochondrial inner membrane, and consequently control cellular ATP levels, mitochondrial Ca^{2+} uptake, and the production of reactive oxygen species. Interest in the development of these and other therapeutic strategies to control various diseases by altering mitochondrial function and signaling has grown significantly in recent years (Murphy and Hartley 2018).

We remark that a key component missing from our model is the role of glycolysis during the three different conditions discussed in this paper. In normal conditions, the ATP consumption by neurons and astrocytes is matched by ATP production from oxidative phosphorylation and glycolysis (94% vs. 6%) (Cohen et al. 1964). However, glycolysis accounts for about 16% of ATP production during SD (Feuerstein et al. 2016) and would most likely play even more prominent role in HSD (Somjen 2001; Lauritzen et al. 2011). Similarly, up to five times increase in glycolysis has been reported during seizure (Wasterlain et al. 2010; Yang et al. 2013). Glycolysis gains further importance when the production of reactive oxygen species and their cytotoxic effects are taken into consideration. These crucial components of mitochondrial function during SZ, SD, and HSD and many related key questions are beyond the scope of this study and the subject of our future research.

Acknowledgements This study was supported by a startup grant from Collage of Arts and Sciences awarded to Ghanim Ullah.

Compliance with Ethical Standards

Conflict of interests The authors declare that they have no conflict of interest.

References

Aiba, I., & Noebels, J.L. (2015). Spreading depolarization in the brainstem mediates sudden cardiorespiratory arrest in mouse sudep models. *Science Translational Medicine*, *7*(282), 282ra46–282ra46.

Aitken, P.G., & Schiff, S.J. (1986). Selective neuronal vulnerability to hypoxia *in vitro*. *Neuroscience Letters*, *67*(1), 92–96.

Aldakkak, M., Stowe, D.F., Heisner, J.S., Spence, M., Camara, A.K. (2008). Enhanced na+/h+ exchange during ischemia and reperfusion impairs mitochondrial bioenergetics and myocardial function. *Journal of Cardiovascular Pharmacology*, *52*(3), 236.

Anderson, T.R., & Andrew, R.D. (2002). Spreading depression: imaging and blockade in the rat neocortical brain slice. *Journal of Neurophysiology*, *88*(5), 2713–2725.

Andersson, B., Aw, T., Jones, D.P. (1987). Mitochondrial transmembrane potential and ph gradient during anoxia. *American Journal of Physiology-Cell Physiology*, *252*(4), C349–C355.

Andrew, R.D., Hsieh, Y.T., Brisson, C.D. (2017). Spreading depolarization triggered by elevated potassium is weak or absent in the rodent lower brain. *Journal of Cerebral Blood Flow & Metabolism*, *37*(5), 1735–1747.

Attwell, D., & Laughlin, S.B. (2001). An energy budget for signaling in the grey matter of the brain. *Journal of Cerebral Blood Flow & Metabolism*, *21*(10), 1133–1145.

Avoli, M., Drapeau, C., Louvel, J., Pumain, R., Olivier, A., Villemure, J.G. (1991). Epileptiform activity induced by low extracellular magnesium in the human cortex maintained *in vitro*. *Annals of Neurology:, Official Journal of the American Neurological Association and the Child Neurology Society*, *30*(4), 589–596.

Ayata, C., & Lauritzen, M. (2015). Spreading depression, spreading depolarizations, and the cerebral vasculature. *Physiological Reviews*, *95*(3), 953–993.

Bahar, S., Fayuk, D., Somjen, G., Aitken, P., Turner, D. (2000). Mitochondrial and intrinsic optical signals imaged during hypoxia and spreading depression in rat hippocampal slices. *Journal of Neurophysiology*, *84*(1), 311–324.

Bahar, S., Suh, M., Zhao, M., Schwartz, T.H. (2006). Intrinsic optical signal imaging of neocortical seizures: the ?epileptic dip?. *Neuroreport*, *17*(5), 499–503.

Bahari, F., Ssentongo, P., Liu, J., Kimbugwe, J., Schiff, S.J., Gluckman, B.J. (2018). Spreading depression and seizure unification experimentally observed in epilepsy. bioRxiv p 455519.

Bayeva, M., Gheorghiade, M., Ardehali, H. (2013). Mitochondria as a therapeutic target in heart failure. *Journal of the American College of Cardiology*, *61*(6), 599–610.

Bikson, M., Hahn, P.J., Fox, J.E., Jefferys, J.G. (2003). Depolarization block of neurons during maintenance of electrographic seizures. *Journal of Neurophysiology*, *90*(4), 2402–2408.

Brisson, C.D., & Andrew, R.D. (2012). A neuronal population in hypothalamus that dramatically resists acute ischemic injury compared to neocortex. *Journal of Neurophysiology*, *108*(2), 419–430.

Brisson, C.D., Lukewich, M.K., Andrew, R.D. (2013). A distinct boundary between the higher brain?s susceptibility to ischemia and the lower brain?s resistance. *PloS One*, *8*(11), e79589.

Camara, A.K., Lesnefsky, E.J., Stowe, D.F. (2010). Potential therapeutic benefits of strategies directed to mitochondria. *Antioxidants & Redox Signaling*, *13*(3), 279–347.

Chang, J.C., Brennan, K.C., He, D., Huang, H., Miura, R.M., Wilson, P.L., Wylie, J.J. (2013). A mathematical model of the metabolic and perfusion effects on cortical spreading depression. *PloS One*, *8*(8), e70469.

Cohen, P., Wollman, H., Alexander, S., Chase, P., Behar, M. (1964). Cerebral carbohydrate metabolism in man during halothane anesthesiaeffects of paco2 on some aspects of carbohydrate utilization. *Anesthesiology:, The Journal of the American Society of Anesthesiologists*, *25*(2), 185–191.

Conte, C., Lee, R., Sarkar, M., Terman, D. (2018). A mathematical model of recurrent spreading depolarizations. *Journal of Computational Neuroscience*, *44*(2), 203–217.

Cressman, J.R., Ullah, G., Ziburkus, J., Schiff, S.J., Barreto, E. (2009). The influence of sodium and potassium dynamics on excitability, seizures, and the stability of persistent states: i. single neuron dynamics. *Journal of Computational Neuroscience*, *26*(2), 159–170.

Czéh, G., Aitken, P.G., Somjen, G.G. (1993). Membrane currents in CA1 pyramidal cells during spreading depression (SD) and SD-like hypoxic depolarization. *Brain Research*, *632*(1-2), 195–208.

Diekman, C.O., Fall, C.P., Lechleiter, J.D., Terman, D. (2013). Modeling the neuroprotective role of enhanced astrocyte mitochondrial metabolism during stroke. *Biophysical Journal*, *104*(8), 1752–1763.

Dreier, J.P. (2011). The role of spreading depression, spreading depolarization and spreading ischemia in neurological disease. *Nature Medicine*, *17*(4), 439.

Dreier, J.P., & Reiffurth, C. (2015). The stroke-migraine depolarization continuum. *Neuron*, *86*(4), 902–922.

Dreier, J.P., Körner, K., Ebert, N., Görner, A., Rubin, I., Back, T., Lindauer, U., Wolf, T., Villringer, A., Einhäupl, K.M., et al. (1998). Nitric oxide scavenging by hemoglobin or nitric oxide synthase inhibition by N-nitro-L-arginine induces cortical spreading ischemia when k^+ is increased in the subarachnoid space. *Journal of Cerebral Blood Flow & Metabolism*, *18*(9), 978–990.

Dreier, J.P., Major, S., Pannek, H.W., Woitzik, J., Scheel, M., Wiesenthal, D., Martus, P., Winkler, M.K., Hartings, J.A., Fabricius, M., et al. (2011). Spreading convulsions, spreading depolarization and epileptogenesis in human cerebral cortex. *Brain: A Journal of Neurology*, *135*(1), 259–275.

Dreier, J.P., Isele, T., Reiffurth, C., Offenhauser, N., Kirov, S.A., Dahlem, M.A., Herreras, O. (2013). Is spreading depolarization characterized by an abrupt, massive release of gibbs free energy from the human brain cortex? *The Neuroscientist*, *19*(1), 25–42.

Dreier, J.P., Fabricius, M., Ayata, C., Sakowitz, O.W., William Shuttleworth, C., Dohmen, C., Graf, R., Vajkoczy, P., Helbok, R., Suzuki, M., et al. (2017). Recording, analysis, and interpretation of spreading depolarizations in neurointensive care: Review and recommendations of the cosbid research group. *Journal of Cerebral Blood Flow & Metabolism*, *37*(5), 1595–1625.

Enger, R., Tang, W., Vindedal, G.F., Jensen, V., Johannes Helm, P., Sprengel, R., Looger, L.L., Nagelhus, E.A. (2015). Dynamics of ionic shifts in cortical spreading depression. *Cerebral Cortex*, *25*(11), 4469–4476.

Fabricius, M., Fuhr, S., Willumsen, L., Dreier, J.P., Bhatia, R., Boutelle, M.G., Hartings, J.A., Bullock, R., Strong, A.J., Lauritzen, M. (2008). Association of seizures with cortical spreading depression and peri-infarct depolarisations in the acutely injured human brain. *Clinical Neurophysiology*, *119*(9), 1973–1984.

Feuerstein, D., Backes, H., Gramer, M., Takagaki, M., Gabel, P., Kumagai, T., Graf, R. (2016). Regulation of cerebral metabolism during cortical spreading depression. *Journal of Cerebral Blood Flow & Metabolism*, *36*(11), 1965–1977.

Friberg, H., & Wieloch, T. (2002). Mitochondrial permeability transition in acute neurodegeneration. *Biochimie*, *84*(2-3), 241–250.

Gabriel, S., Njunting, M., Pomper, J.K., Merschhemke, M., Sanabria, E.R., Eilers, A., Kivi, A., Zeller, M., Meencke, H.J., Cavalheiro, E.A., et al. (2004). Stimulus and potassium-induced epileptiform

activity in the human dentate gyrus from patients with and without hippocampal sclerosis. *Journal of Neuroscience*, *24*(46), 10416–10430.

Galeffi, F., Somjen, G.G., Foster, K.A., Turner, D.A. (2011). Simultaneous monitoring of tissue po2 and nadh fluorescence during synaptic stimulation and spreading depression reveals a transient dissociation between oxygen utilization and mitochondrial redox state in rat hippocampal slices. *Journal of Cerebral Blood Flow & Metabolism*, *31*(2), 626–639.

Gault, L.M., Lin, C.W., LaManna, J.C., Lust, W.D. (1994). Changes in energy metabolites, cgmp and intracellular ph during cortical spreading depression. *Brain Research*, *641*(1), 176–180.

Gloor, S.M. (1997). Relevance of Na,$k-ATPase$ to local extracellular potassium homeostasis and modulation of synaptic transmission. *FEBS Letters*, *412*(1), 1–4.

Gloveli, T., Dugladze, T., Saha, S., Monyer, H., Heinemann, U., Traub, R.D., Whittington, M.A., Buhl, E.H. (2005). Differential involvement of oriens/pyramidale interneurones in hippocampal network oscillations *in vitro*. *The Journal of Physiology*, *562*(1), 131–147.

Grinberg, Y.Y., van Drongelen, W., Kraig, R.P. (2012). Insulin-like growth factor-1 lowers spreading depression susceptibility and reduces oxidative stress. *Journal of Neurochemistry*, *122*(1), 221–229.

Grinberg, Y.Y., Dibbern, M.E., Levasseur, V.A., Kraig, R.P. (2013). Insulin-like growth factor-1 abrogates microglial oxidative stress and TNF-α responses to spreading depression. *Journal of Neurochemistry*, *126*(5), 662–672.

Hablitz, J.J., & Heinemann, U. (1989). Alterations in the microenvironment during spreading depression associated with epileptiform activity in the immature neocortex. *Developmental Brain Research*, *46*(2), 243–252.

Hansen, A. (1984). The role of spreading depression in acute brain disorders. *Anais da Academia Brasileira de Ci?ncias*, *56*, 457–479.

Hansen, A.J., & Zeuthen, T. (1981). Extracellular ion concentrations during spreading depression and ischemia in the rat brain cortex. *Acta Physiologica*, *113*(4), 437–445.

Hartings, J.A., Shuttleworth, C.W., Kirov, S.A., Ayata, C., Hinzman, J.M., Foreman, B., Andrew, R.D., Boutelle, M.G., Brennan, K., Carlson, A.P., et al. (2017). The continuum of spreading depolarizations in acute cortical lesion development: examining leão?s legacy. *Journal of Cerebral Blood Flow & Metabolism*, *37*(5), 1571–1594.

Hawrysh, P.J., & Buck, L.T. (2019). Mitochondrial matrix ph acidifies during anoxia and is maintained by the f1f0-atp ase in anoxia-tolerant painted turtle cortical neurons. FEBS Open Bio pp. https://doi.org/10.1002/2211–5463.12612.

Hazelton, J.L., Petrasheuskaya, M., Fiskum, G., Kristián, T. (2009). Cyclophilin d is expressed predominantly in mitochondria of γ-aminobutyric acidergic interneurons. *Journal of Neuroscience Research*, *87*(5), 1250–1259.

Homer, L.D., Shelton, J.B., Williams, T.J. (1983). Diffusion of oxygen in slices of rat brain. *American Journal of Physiology-Regulatory, Integrative and Comparative Physiology*, *244*(1), R15–R22.

Hosseini-Zare, M.S., Gu, F., Abdulla, A., Powell, S., Žiburkus, J. (2017). Effects of experimental traumatic brain injury and impaired glutamate transport on cortical spreading depression. *Experimental Neurology*, *295*, 155–161.

Hübel, N., & Dahlem, M.A. (2014). Dynamics from seconds to hours in hodgkin-huxley model with time-dependent ion concentrations and buffer reservoirs. *PLos Computational Biology*, *10*(12), e1003941.

Hübel, N., & Ullah, G. (2016). Anions govern cell volume: a case study of relative astrocytic and neuronal swelling in spreading depolarization. *Plos One*, *11*(3), e0147060.

Hübel, N., Andrew, R.D., Ullah, G. (2016). Large extracellular space leads to neuronal susceptibility to ischemic injury in a na+/k+ pumps–dependent manner. *Journal of Computational Neuroscience*, *40*(2), 177–192.

Hübel, N., Hosseini-Zare, M.S., Žiburkus, J., Ullah, G. (2017). The role of glutamate in neuronal ion homeostasis: A case study of spreading depolarization. *PLos Computational Biology*, *13*(10), e1005804.

Ingram, J.M., Zhang, C., Xu, J., Schiff, S.J. (2013). Fret excited ratiometric oxygen sensing in living tissue. *Journal of Neuroscience Methods*, *214*(1), 45–51.

Jing, J., Aitken, P.G., Somjen, G.G. (1994). Interstitial volume changes during spreading depression (SD) and SD-like hypoxic depolarization in hippocampal tissue slices. *Journal of Neurophysiology*, *71*(6), 2548–2551.

Jitschin, R., Hofmann, A.D., Bruns, H., Gießl, A., Bricks, J., Berger, J., Saul, D., Eckart, M.J., Mackensen, A., Mougiakakos, D. (2014). Mitochondrial metabolism contributes to oxidative stress and reveals therapeutic targets in chronic lymphocytic leukemia. *Blood*, *123*(17), 2663–2672.

Kager, H., Wadman, W., Somjen, G. (2000). Simulated seizures and spreading depression in a neuron model incorporating interstitial space and ion concentrations. *Journal of Neurophysiology*, *84*(1), 495–512.

Kager, H., Wadman, W., Somjen, G. (2002). Conditions for the triggering of spreading depression studied with computer simulations. *Journal of Neurophysiology*, *88*(5), 2700–2712.

Kager, H., Wadman, W., Somjen, G. (2007). Seizure-like after discharges simulated in a model neuron. *Journal of Computational Neuroscience*, *22*(2), 105–128.

Köhling, R., Koch, U., Hagemann, G., Redecker, C., Straub, H., Speckmann, E.J. (2003). Differential sensitivity to induction of spreading depression by partial disinhibition in chronically epileptic human and rat as compared to native rat neocortical tissue. *Brain Research*, *975*(1-2), 129–134.

Kovács, R., Schuchmann, S., Gabriel, S., Kann, O., Kardos, J., Heinemann, U. (2002). Free radical–mediated cell damage after experimental status epilepticus in hippocampal slice cultures. *Journal of Neurophysiology*, *88*(6), 2909–2918.

Kovács, R., Kardos, J., Heinemann, U., Kann, O. (2005). Mitochondrial calcium ion and membrane potential transients follow the pattern of epileptiform discharges in hippocampal slice cultures. *Journal of Neuroscience*, *25*(17), 4260–4269.

Krishnan, G.P., & Bazhenov, M. (2011). Ionic dynamics mediate spontaneous termination of seizures and postictal depression state. *Journal of Neuroscience*, *31*(24), 8870–8882.

Lauf, P.K., & Adragna, N.C. (2000). K − Cl cotransport: properties and molecular mechanism. *Cellular Physiology and Biochemistry*, *10*(5-6), 341–354.

Lauritzen, M., Dreier, J.P., Fabricius, M., Hartings, J.A., Graf, R., Strong, A.J. (2011). Clinical relevance of cortical spreading depression in neurological disorders: migraine, malignant stroke, subarachnoid and intracranial hemorrhage, and traumatic brain injury. *Journal of Cerebral Blood Flow & Metabolism*, *31*(1), 17–35.

Lee, B.H., Seo, H.W., Yi, K.Y., Lee, S., Lee, S., Yoo, S.E. (2005). Effects of kr-32570, a new na+/h+ exchanger inhibitor, on functional and metabolic impairments produced by global ischemia and reperfusion in the perfused rat heart. *European Journal of Pharmacology*, *511*(2-3), 175–182.

Lennie, P. (2003). The cost of cortical computation. *Current Biology*, *13*(6), 493–497.

Li, Y.X., & Rinzel, J. (1994). Equations for $insp_3$ receptor-mediated $[Ca^{2+}]_i$ oscillations derived from a detailed kinetic model: a hodgkin-huxley like formalism. *Journal of Theoretical Biology*, *166*(4), 461–473.

Lipton, P. (1999). Ischemic cell death in brain neurons. *Physiological Reviews*, *79*(4), 1431–1568.

Liu, F., Lu, J., Manaenko, A., Tang, J., Hu, Q. (2018). Mitochondria in ischemic stroke: New insight and implications. *Aging and Disease*, *9*(5), 924.

Lothman, E., LaManna, J., Cordingley, G., Rosenthal, M., Somjen, G. (1975). Responses of electrical potential, potassium levels, and oxidative metabolic activity of the cerebral neocortex of cats. *Brain Research*, *88*(1), 15–36.

Magnus, G., & Keizer, J. (1997). Minimal model of beta-cell mitochondrial Ca^{2+} handling. *American Journal of Physiology. Cell Physiology*, *273*(2), C717–C733.

Major, S., Petzold, G.C., Reiffurth, C., Windmüller, O., Foddis, M., Lindauer, U., Kang, E.J., Dreier, J.P. (2017). A role of the sodium pump in spreading ischemia in rats. *Journal of Cerebral Blood Flow & Metabolism*, *37*(5), 1687–1705.

Mayevsky, A., Zarchin, N., Friedli, C.M. (1982). Factors affecting the oxygen balance in the awake cerebral cortex exposed to spreading depression. *Brain Research*, *236*(1), 93–105.

Mody, I., Lambert, J., Heinemann, U. (1987). Low extracellular magnesium induces epileptiform activity and spreading depression in rat hippocampal slices. *Journal of Neurophysiology*, *57*(3), 869–888.

Murphy, M.P., & Hartley, R.C. (2018). Mitochondria as a therapeutic target for common pathologies. Nature Reviews Drug Discovery.

Nicholls, D.G., & Budd, S.L. (2000). Mitochondria and neuronal survival. *Physiological Reviews*, *80*(1), 315–360.

Østby, I., Øyehaug, L., Einevoll, G.T., Nagelhus, E.A., Plahte, E., Zeuthen, T., Lloyd, C.M., Ottersen, O.P., Omholt, S.W. (2009). Astrocytic mechanisms explaining neural-activity-induced shrinkage of extraneuronal space. *PLos Computational Biology*, *5*(1), e1000272.

Øyehaug, L., Østby, I., Lloyd, C.M., Omholt, S.W., Einevoll, G.T. (2012). Dependence of spontaneous neuronal firing and depolarisation block on astroglial membrane transport mechanisms. *Journal of Computational Neuroscience*, *32*(1), 147–165.

Payne, J.A., Rivera, C., Voipio, J., Kaila, K. (2003). Cation–chloride co-transporters in neuronal communication, development and trauma. *Trends in Neurosciences*, *26*(4), 199–206.

Piilgaard, H., Witgen, B.M., Rasmussen, P., Lauritzen, M. (2011). Cyclosporine a, FK506, and NIM811 ameliorate prolonged cbf reduction and impaired neurovascular coupling after cortical spreading depression. *Journal of Cerebral Blood Flow & Metabolism*, *31*(7), 1588–1598.

Pomper, J.K., Haack, S., Petzold, G.C., Buchheim, K., Gabriel, S., Hoffmann, U., Heinemann, U. (2006). Repetitive spreading depression-like events result in cell damage in juvenile hippocampal slice cultures maintained in normoxia. Journal of Neurophysiology.

Rosenthal, M., & Martel, D.L. (1979). Ischemia-induced alterations in oxidative ?recovery? metabolism after spreading cortical depression in situ. *Experimental Neurology*, *63*(2), 367–378.

Russo, E., Nguyen, H., Lippert, T., Tuazon, J., Borlongan, C.V., Napoli, E. (2018). Mitochondrial targeting as a novel therapy for stroke. *Brain Circulation*, *4*(3), 84.

Scanlon, J., Brocard, J., Stout, A., Reynolds, I. (2000). Pharmacological investigation of mitochondrial Ca^{2+} transport in central neurons: studies with CGP-37157, an inhibitor of the mitochondrial na^{+}–Ca^{2+} exchanger. *Cell Calcium*, *28*(5-6), 317–327.

Schechter, M., Sonn, J., Mayevsky, A. (2009). Brain oxygen balance under various experimental pathophysiologycal conditions. In *Oxygen Transport to Tissue* (pp. 293–299). Berlin: Springer.

Schild, L., Blair, P.V., Davis, W.I., Baugh, S. (1999). Effect of adenine nucleotide pool size in mitochondria on intramitochondrial ATP levels. *Biochimica et Biophysica Acta (BBA)-Bioenergetics*, *1413*(1), 14–20.

Somjen, G.G. (2001). Mechanisms of spreading depression and hypoxic spreading depression-like depolarization. *Physiological Reviews*, *81*(3), 1065–1096.

Somjen, G.G. (2004). Ions in the brain New york: Oxford UP.

Sonn, J., & Mayevsky, A. (2000). Effects of brain oxygenation on metabolic, hemodynamic, ionic and electrical responses to spreading depression in the rat. *Brain Research*, *882*(1-2), 212–216.

Syková, E., & Nicholson, C. (2008). Diffusion in brain extracellular space. *Physiological Reviews*, *88*(4), 1277–1340.

Toglia, P., & Ullah, G. (2016). The gain-of-function enhancement of IP_3-receptor channel gating by familial Alzheimer′s disease-linked presenilin mutants increases the open probability of mitochondrial permeability transition pore. *Cell Calcium*, *60*(1), 13–24.

Toglia, P., Cheung, K.H., Mak, D.O.D., Ullah, G. (2016). Impaired mitochondrial function due to familial Alzheimer′s disease-causing presenilins mutants via Ca^{2+} disruptions. *Cell Calcium*, *59*(5), 240–250.

Toglia, P., Demuro, A., Mak, D.O.D., Ullah, G. (2018). Data-driven modeling of mitochondrial dysfunction in alzheimer's disease. *Cell Calcium*, *76*, 23–35.

Traub, R.D., Jefferys, J., Miles, R., Whittington, M.A., Tóth, K. (1994). A branching dendritic model of a rodent CA3 pyramidal neurone. *The Journal of Physiology*, *481*(1), 79–95.

Traynelis, S.F., & Dingledine, R. (1988). Potassium-induced spontaneous electrographic seizures in the rat hippocampal slice. *Journal of Neurophysiology*, *59*(1), 259–276.

Ullah, G., Jung, P., Cornell-Bell, A.H. (2006). Anti-phase calcium oscillations in astrocytes via inositol (1, 4, 5)-trisphosphate regeneration. *Cell Calcium*, *39*(3), 197–208.

Ullah, G., Cressman, J.R. Jr., Barreto, E., Schiff, S.J. (2009). The influence of sodium and potassium dynamics on excitability, seizures, and the stability of persistent states: Ii. network and glial dynamics. *Journal of Computational Neuroscience*, *26*(2), 171–183.

Ullah, G., Wei, Y., Dahlem, M.A., Wechselberger, M., Schiff, S.J. (2015). The role of cell volume in the dynamics of seizure, spreading depression, and anoxic depolarization. *PLos Computational Biology*, *11*(8), e1004414.

Vaillend, C., Mason, S.E., Cuttle, M.F., Alger, B.E. (2002). Mechanisms of neuronal hyperexcitability caused by partial inhibition of na+-k+-atpases in the rat ca1 hippocampal region. *Journal of Neurophysiology*, *88*(6), 2963–2978.

Wacquier, B., Combettes, L., Van Nhieu, G.T., Dupont, G. (2016). Interplay between intracellular Ca^{2+} oscillations and Ca^{2+}-stimulated mitochondrial metabolism. *Scientific Reports*, *6*, 19316.

Waldmeier, P.C., Feldtrauer, J.J., Qian, T., Lemasters, J.J. (2002). Inhibition of the mitochondrial permeability transition by the non-immunosuppressive cyclosporin derivative NIM811. *Molecular Pharmacology*, *62*(1), 22–29.

Wang, J., Chambers, G., Cottrell, J., Kass, I. (2000). Differential fall in ATP accounts for effects of temperature on hypoxic damage in rat hippocampal slices. *Journal of Neurophysiology*, *83*(6), 3462–3472.

Wasterlain, C.G., Thompson, K.W., Suchomelova, L., Niquet, J. (2010). Brain energy metabolism during experimental neonatal seizures. *Neurochemical Research*, *35*(12), 2193–2198.

Wei, Y., Ullah, G., Ingram, J., Schiff, S.J. (2014a). Oxygen and seizure dynamics: II. computational modeling. *Journal of Neurophysiology*, *112*(2), 213–223.

Wei, Y., Ullah, G., Schiff, S.J. (2014b). Unification of neuronal spikes, seizures, and spreading depression. *Journal of Neuroscience*, *34*(35), 11733–11743.

Yang, H., Wu, J., Guo, R., Peng, Y., Zheng, W., Liu, D., Song, Z. (2013). Glycolysis in energy metabolism during seizures. *Neural Regeneration Research*, *8*(14), 1316.

Zhang, Y., & Lipton, P. (1999). Cytosolic Ca^{2+} changes during in vitroischemia in rat hippocampal slices: Major roles for glutamate and na^{+}-dependent Ca^{2+} release from mitochondria. *Journal of Neuroscience*, *19*(9), 3307–3315.

Zhou, N., Gordon, G.R., Feighan, D., MacVicar, B.A. (2010). Transient swelling, acidification, and mitochondrial depolarization occurs in neurons but not astrocytes during spreading depression. *Cerebral Cortex*, *20*(11), 2614–2624.